Doctoral Dissertation
博士論文

Identification and Functional Analysis of Genes Critical to Tumorigenesis
（腫瘍形成に必須な遺伝子の同定と機能解析）

A Dissertation Submitted for the Degree of Doctor of Philosophy

July 2020
令和 2 年 7 月博士（理学）申請

Department of Biology, Graduate School of Science,
The University of Tokyo
東京大学大学院理学系研究科生物科学専攻

Brandon James Cona
コウナ　ブランドン　ジェームズ

Table of Contents

Abstract

The mechanisms by which a given population of cells acquires neoplastic features are generally considered to be a direct result of the mutations present in those cells. However, certain cancers, such as ovarian clear cell carcinoma (OCCC), display high levels of genetic variation between patients, making it difficult to fully grasp the mechanisms underlying its tumorigenesis, and subsequently confounding the development of effective therapies. In chapter 1, in order to identify genes critical to the growth of OCCC, I carried out a comprehensive CRISPR-Cas9 knockout screen against cell growth using an OCCC cell line, JHOC5, with none of the mutations hallmark to OCCC, as well as a normal ovarian surface epithelium cell line, OSE3, as a control. After comparing my data with publically available datasets, I identified DHX38 as a gene critical for the growth of OCCC. Finally, in chapter 2, it was discovered that DHX38 knockdown causes OCCC cells to undergo apoptosis in a p53 stabilization-independent manner. It was also discovered that DHX38 binds to several proteins implicated in the regulation of apoptosis. Taken together, these results suggest that DHX38 may play a role in OCCC tumorigenesis, and can be regarded as a promising therapeutic target.

Table of Abbreviations

Abbreviation	Full Name
AML	Acute Myeloid Leukemia
APAF-1	Apoptotic Protease Activating Factor 1
ARID1A	AT-Rich Interaction Domain 1A
ATM	Ataxia telangiectasia Mutated
ATR	Ataxia telangiectasia and Rad3 Related
Akt	Protein Kinase B
CARD	Caspase Recruitment Domain
CBP	CREB-Binding Protein
DHX38	DEAH-Box Helicase 38
DSB	Double Strand Break
EMT	Epithelial-Mesenchymal Transition
ERK	Extracellular Signal-Regulated Kinase
GeCKO	Genome-Scale CRISPR Knock-Out
HDAC6	Histone Deacetylase 6
HDR	Homology-Directed Repair
IKK	IkB kinase
IkB	Inhibitor of Nuclear Factor Kappa B
KRAS	Kirsten Rat Sarcoma Virus
MAGeCK	Model-Based Analysis of Genome-wide CRISPR-Cas9 Knockout
MDM2	Mouse Double Minute 2 Homolog
mTOR	Mammalian Target of Rapamycin

NFkB	Nuclear Factor-Kappa B
NHEJ	Non-Homologous End Joining
NOXA	NADPH Oxidase Activator 1
OCCC	Ovarian Clear Cell Carcinoma
PI3K	Phosphoinositide 3-Kinase
PIK3CA	Phosphatidylinositol-4,5-Bisphosphate 3-Kinase Catalytic Subunit Alpha
PUMA	p53 Upregulated Modulator of Apoptosis
RRA	Robust Rank Aggregation
SWI/SNF	Switch/Sucrose Non-Fermentable
TNF α	Tumor Necrosis Factor Alpha
TNFR	Tumor Necrosis Factor Receptor

General Introduction

Cancer is a multi-faceted disease whose effective treatment relies on the exploitation of its addiction to certain gene products. These gene products lead to several of cancer cells' signature characteristics such as increased proliferation, the ability to evade the body's immune system, and avoidance of certain built-in regulatory mechanisms such as apoptosis. Many next-generation cancer therapies would not exist without knowledge of the gene products a given cancer is addicted to. This knowledge can often be gleamed from irregularities in the complex signaling pathways at work in a given cancer cell, generated from its accumulation of mutations. For example, colorectal cancer cells often show activating mutations in the kirsten rat sarcoma virus (KRAS) gene, which lead to increased proliferation and Epithelial-Mesenchymal Transition (EMT) (Shao et al., 2014; Singh et al., 2009). By targeting this overactive KRAS and its downstream factors, promising new therapies have been developed (Liu et al., 2019; Zhu et al., 2014). However, it is not always immediately obvious what genes a given cancer is addicted to. Even when considering mutations along pathway lines, certain cancer types show a surprising amount of variability in their mutation patterns. One such cancer is Ovarian Clear Cell Carcinoma (OCCC). While just over half of all OCCC cases present with activating mutations in the protein kinase B (Akt) / extracellular signal-regulated kinase (ERK) / mammalian target of rapamycin (mTOR) pathway and/or inactivating mutations in members of the SWItch / Sucrose Non-Fermentable (SWI/SNF) complex as per the COSMIC Catalogue of Somatic Mutations in Cancer (Tate et al., 2018), the remaining cases show no such uniformity. Particularly in Japan, the proper treatment of OCCC is a large problem, owing not only

to the 8% efficacy traditional treatment methods show against its higher staged cases, but also because the incidence rate of OCCC in Japan and other Asian countries is over double that of the west (Anglesio et al., 2011; Crotzeret al., 2007; Mabuchi et al., 2016; Sugiyama et al., 2000). The goal of my research is to better understand the genes that OCCC is addicted to, in order to allow for the development of novel therapies against it.

Chapter I

CRISPR-Cas9 Knockout Screening

Introduction

In chapter I, I carry out a CRISPR-Cas9 screen against an ovarian clear cell carcinoma cell line and a normal ovarian surface epithelium cell line, in order to uncover genes essential for ovarian clear cell carcinoma cell growth. I then employ an analysis of publicly available data in order to narrow down my screening results to a single gene on which to carry out functional analysis.

Ovarian Clear Cell Carcinoma

Epithelial ovarian cancer can be divided into five histological subtypes: serous, mucinous, endometrial, undifferentiated, and clear cell, with an average 5-year survival rate of 58.0% according to recent data from the Japan National Cancer Center. Of these, the clear cell subtype (OCCC) shows particularly poor prognoses, with higher-stage OCCC tumors presenting with severely low 5-year survival rates of between 20% and 30% (Ku et al., 2018; Tang et al., 2018). One of the major reasons for these poor prognoses is the poor response OCCC tumors have to conventional therapies. While the exact numbers vary between 1% and 8% depending on the study, conventional platinum-based therapies have extremely poor efficacy against advanced cases (Crotzeret al., 2007; Sugiyama et al., 2000). Additionally, the incidence rate of the clear cell carcinoma subtype in Asian countries, including Japan, has been found to be over double that of the west, at between 23% and 25% of all epithelial ovarian cancer cases (Anglesio et al., 2011).

One of the challenges in the development of therapies targeted to OCCC is that

mutations in OCCC tumors are highly diverse. In only around half of cases does there exist a common mutational signature: ARID1A (AT-Rich Interaction Domain 1A) loss-of-function mutations and/or PIK3CA (Phosphatidylinositol-4,5-Bisphosphate 3-Kinase Catalytic Subunit Alpha) gain-of-function mutations (Tate et al., 2018). ARID1A is a member of the BAF subclass of the human SWI/SNF (Switch/Sucrose Non-Fermentable) complex, which acts as an antagonist to the polycomb repressor complex in that it modifies histones to allow for the relaxation of condensed chromatin thereby increasing transcriptional activity at a given genetic locus (Bracken et al., 2019). ARID1A has also been shown to bind to ATR (Ataxia telangiectasia and Rad3 Related) at double strand break (DSB) sites to promote non-homologous end joining (NHEJ) by recruiting Ku70 and Ku80, and induced missense mutations have been shown to be sufficient to impair G2/M checkpoint control after induction of DSBs through irradiation, suggesting that ARID1A may also play a role in detection of DSBs (Shen et al., 2015; Watanabe et al., 2014). Additionally, loss of ARID1A has been shown to upregulate the expression of histone deacetylase 6 (HDAC6), which acetylates p53 at Lys-20 and promotes its transcriptional activity (Bitler et al., 2018).

In OCCC and colorectal carcinoma cells, ARID1A loss was also shown to facilitate the expression of genes involved in the phosphoinositide 3-kinase (PI3K)/AKT/mTOR signaling cascade, to which the second most frequently mutated gene in OCCC, PIK3CA, belongs (Samartzis et al., 2014). In normal cells, the PI3K/Akt signaling pathways is one of many pathways responsible for transducing extracellular signals – mainly those related to promoting metabolism, survival, growth and proliferation, motility, translation, and angiogenesis – in a controlled manner through the phosphorylation of downstream factors (Yang et al., 2019). However, through the

introduction of activating mutations, PIK3CA can morph into a constitutively active oncogenic form; as such, activating mutations in PIK3CA are seen in a wide range of cancers, not just in OCCC, but also in colorectal, breast, liver, lung, and brain cancers (Hamada et al., 2017; Kim et al., 2013; McNeill et al., 2018; Mosele et al., 2020; Yamamoto et al., 2008).

Knockout of both of these genes in tandem, but not individually, has been shown to induce ovarian hyperplasia and subsequent tumorigenesis with a similar histology to human OCCC in a mouse model (Chandler et al., 2015). However, in just under half of OCCC cases, mutations in members of neither the PI3K/AKT/mTOR cascade nor the SWI/SNF complex are observed, and so aberrations in the PI3K/AKT/mTOR pathway and SWI/SNF complex alone are insufficient to fully describe the mechanisms underlying OCCC tumorigenesis. In addition, there is no overarching mutational signature present in these remaining cases, underscoring the fact that current understanding of the physiological signaling pathways underpinning OCCC tumorigenesis and progression is insufficient. In the present study, with the goal to elucidate novel mechanisms behind OCCC tumorigenesis and progression, I set out to identify in OCCC genes critical to one of the most characteristic properties of cancer – the dysregulation of cell growth.

Materials and Methods

Cell Culture

JHOC5 ovarian clear cell carcinoma cells, OSE3 normal ovarian surface epithelium cells, and PC3 prostate adenocarcinoma cells were cultured in RPMI1640 medium supplemented with 10% fetal bovine serum (FBS) and 2 mM L-glutamine. HEK293FT human embryonic kidney cells and A549 lung carcinoma cells were cultured in DMEM medium supplemented with 10% FBS and 4 mM L-glutamine. All cell lines were cultured at 37°C under a 5% CO_2 atmosphere.

Growth Assays

Cell growth was assayed using the Cell-Titer Glo Luminescent Cell Viability Assay (Promega). After removing culture medium, cells were washed once with PBS, and an appropriate amount of Cell-Titer Glo Reagant diluted 4x in PBS was added. Plates were then shaken at room temperature for 10 minutes, after which fluorescence was measured using a Mithras LB 940 Plate Reader (BERTHOLD).

Viral Construction

The lentiCas9-Blast and lentiGuide-Puro two vector system was purchased from Addgene and prepared following the manufacturer's instructions. Lentiviruses were prepared via cotransfection of HEK293FT cells with the appropriate vector along with the packaging plasmids psPAX2 and pMD2.G using polyethylenimine 'MAX' (PEI, Polyscience, Inc. Cat. 24765) in a 4:6 mix of OPTIMEM:DMEM, and collected via ultracentrifugation after 72 hours.

Viral Transfection and CRISPR-Cas9 Screening

Cells were first infected with a lentivirus containing the lentiCas9-Blast vector at a multiplicity of infection (MOI) of 0.3. After selection for four days with an appropriate concentration of blasticidin, 1.85 x 10^7 cells were next infected with a lentivirus containing the lentiGuide-Puro library A vector at an MOI of 0.3 to ensure an average coverage of over 300 cells per sgRNA, and selection was carried out for 3 days in the same way as above with puromycin. A sample of 2 x 10^7 cells was pelleted and frozen under liquid nitrogen to be used as a Day 0 sample. Cells were then passaged continuously until they had undergone 8 doublings, as determined by counting in between passages. To maintain sufficient sgRNA coverage, the total number of cells was maintained above 2 x 10^7 for the duration of the culture period. After cells had undergone 10 doublings, a second sample of 2 x 10^7 cells was taken as a final time point.

Genomic DNA Extraction, PCR, and Library Amplification and Sequencing

Genomic DNA was extracted from the above mentioned samples using the QIAGEN Blood and Cell Culture DNA Midi Kit. Subsequently, 125µg of genomic DNA from each sample was split into 2.5 µg fractions and sgRNA sequences were amplified to form a sequencing library in two steps. The first PCR was used to amplify the sgRNA-containing genomic sequence and append adapters (shown below) for use in attaching sequencing barcodes, and was carried out in 30 cycles. The second PCR was used to attach sequencing barcodes (primers shown below), and was carried out in 30 cycles, with 5µL of the first PCR reaction products used in each 50µL reaction. Both PCRs were carried out using the Herculase II Fusion DNA Polymerase from Agilent

following the manufacturer's instructions, after which the library was purified on a 2% agarose gel, extracted using the QIAquick Gel Extraction Kit (QIAGEN), measured for fragment size using the 2200 Tapestation (Agilent), and quantified using the KAPA SYBR Fast qPCR Kit (KAPA BIOSYSTEMS). Libraries were sequenced on a HiSeq2500 (Illumina).

First PCR Primers

Forward Primer:
AATGGACTATCATATGCTTACCGTAACTTGAAAGTATTTCG
Reverse Primer:
TCTACTATTCTTTCCCCTGCACTGTTGTGGGCGATGTGCGCTCTG

Second PCR Primers

Forward Primer #06:
5'-AATGATACGGCGACCACCGAGATCTACACTCTTTCCCTACACGACGCTCTT
CCGATCTatcgattcttgtggaaaggacgaaacaccg-3'
Forward Primer #08:
5'-AATGATACGGCGACCACCGAGATCTACACTCTTTCCCTACACGACGCTCTT
CCGATCTcgatcgattcttgtggaaaggacgaaacaccg-3'
Forward Primer #09:
5'-AATGATACGGCGACCACCGAGATCTACACTCTTTCCCTACACGACGCTCTT
CCGATCTacgatcgattcttgtggaaaggacgaaacaccg-3'
Forward Primer #10:
5'-AATGATACGGCGACCACCGAGATCTACACTCTTTCCCTACACGACGCTCTT
CCGATCTttcttgtggaaaggacgaaacaccg-3'
Reverse Primer #01:
5'-CAAGCAGAAGACGGCATACGAGATCGTGATGTGACTGGAGTTCAGACGTG

TGCTCTTCCGATCTTCTACTATTCTTTCCCCTGCACTGT-3’

Reverse Primer #03:

5’-CAAGCAGAAGACGGCATACGAGATTCAAGTGTGACTGGAGTTCAGACGT GTGCTCTTCCGATCTTCTACTATTCTTTCCCCTGCACTGT-3’

Reverse Primer #05:

5’-CAAGCAGAAGACGGCATACGAGATAAGCTAGTGACTGGAGTTCAGACGTG TGCTCTTCCGATCTTCTACTATTCTTTCCCCTGCACTGT-3’

Reverse Primer #07:

5’-CAAGCAGAAGACGGCATACGAGATGGCCACGTGACTGGAGTTCAGACGT

GTGCTCTTCCGATCTTCTACTATTCTTTCCCCTGCACTGT-3’

siRNA Transfection

For siRNA-based validation experiments, adherent cells were trypsinized and dissociated from plates. Lipofectamine RNAiMAX Transfection Reagent (Invitrogen) was diluted in Opti-MEM I reduced serum medium (Opti-MEM) such that it would have a final concentration in the transfection medium of 1% v/v, and allowed to equilibrate briefly. Separately, siRNA oligomers purchased from Ambion were diluted in Opti-MEM such that their final concentration in the transfection medium was 10 nM. The equilibrated RNAiMAX solution and an equal volume of diluted siRNA solution were mixed, vortexed, and allowed to incubate at room temperature for 20 minutes. At the end of the incubation period, an appropriate volume (1 part) of transfection medium was added per well, followed by an appropriate volume (5 parts) and density of dissociated cells.

siRNA catalogue numbers are as shown below:

Negative Control #1 siRNA (catalogue #4390844)

siPLK1#1,#2: s448, s449

siDHX38#1-#3: s18906, s18908, s18907

siDDX42#1-#3: s22329, s22328, s22330

siPPP2CA#1-#3: s10957, s10958, s10959

siDARS#1-#3: s3932, s223380, s3933

RNA Extraction and Reverse Transcription

Total RNA was extracted from cells and purified using TRIsure (BIOLINE) following the manufacturer's protocol, using 1mL of reagent per 1 x 10^6 cells. RNA pellets were resuspended in MilliQ and stored at -80°C. Synthesis of cDNA was carried out using Prime Script RT Master Mix (TaKaRa).

Statistical Analysis

Statistical analysis was performed using R version 3.6.0 (http://www.r-project.org/).

Results

In order to identify cancer-specific genetic growth dependencies in OCCC, I carried out a clustered regularly interspaced short palindromic repeat (CRISPR)-Cas9 knockout screening, based on the CRISPR-Cas9 system (Shalem et al., 2013). In recent years, the CRISPR-Cas9 system has come to prominence as the leading tool for in-vitro and in-vivo gene editing. In this system, which is based on an innate bacterial immune defense system against bacteriophages, the DNA-cleaving Cas9 protein is introduced into cells along with a single-guide RNA (sgRNA) targeting the gene of interest. The sgRNA acts as a template which binds both the Cas9 protein as well as any DNA sequences in the cell that show reverse-complementary to a 21-bp stretch at its 5', with the condition that a specific 3-bp sequence (called the PAM sequence) – differing among bacterial species – is present at the 3' end of the DNA strand complementary to the sgRNA recognition sequence. Using this technology with designer sgRNAs allows for the introduction of double strand breaks almost anywhere in the genome, and by taking advantage of the cell's innate repair machinery [NHEJ+ HDR (homology-directed repair)] one can not only introduce mutations, but also whole expression cassettes and even large deletions.

Cells were screened using the Genome-scale CRISPR Knock-Out (GeCKO) v2 2-vector CRISPR-Cas9 knockout screening system (Fig. 1) (Sanjana et al., 2015). A population of cells was first infected with two viruses, containing expression cassettes for the Cas9 protein and a comprehensive sgRNA library targeting roughly 20,000 human genes with 3 sgRNAs per coding gene and 4 sgRNAs per miRNA. Cells were infected in such a way that each received a single copy of the Cas9 gene, as well as a

single plasmid from the sgRNA library, and each sgRNA had an average coverage of at least 300 cells. Cells were then passaged until they had doubled 8 times. In this way, the growth of cells containing sgRNA expression cassettes targeting genes critical for cell growth would be inhibited. As this translates to a decrease in the relative percentage of cells containing that sgRNA over the course of the culture period, by taking a sample before and after the culture period and calculating the degree of change in sgRNA representation, one can identify genes critical for cell growth in that cell line. As the GeCKO v2 2-vector CRISPR-Cas9 knockout screening library A contains 3 sgRNAs targeted to each human coding gene and 4 sgRNAs targeted to each miRNA, I used the Model-based Analysis of Genome-wide CRISPR-Cas9 Knockout (MAGeCK) Robust Rank Aggregation (RRA) tool to aggregate depletion data across multiple sgRNAs targeting the same gene (Li et al., 2014). This gave an overall depletion score for each coding gene and miRNA with an associated p-value.

In order to identify potential dependencies in OCCC tumors containing none of the common mutations present in roughly half of OCCC cases, I screened the JHOC5 cell line, which does not contain any of the aforementioned mutations. Additionally, to identify cancer-specific dependencies, I also screened the OSE3 cell line; a normal ovarian surface epithelium cell line immortalized using the SV40 T Antigen. Comparing screening results between JHOC5 and OSE3 cell lines, I was able to identify 462 genes whose targeting sgRNAs were significantly ($p<0.02$) depleted in JHOC5 cells after the growth period, compared to 535 genes in OSE3 cells (Fig. 2, 3). Of these genes, 52 were common among both JHOC5 and OSE3. Statistical overrepresentation analysis on the JHOC5-specific growth-critical genes using the GO-slim biological function panther classification system ontologies (Mi et al., 2010; Thomas et al., 2003) identified 9

significantly enriched ($p < 0.01$) ontologies, of which four were related to mRNA splicing (Fig. 4).

Of the gene ontologies determined to be enriched in the JHOC5/OSE3 screening candidate gene dataset, those related to mRNA splicing contained 11 genes (Table 1). In order to confirm that these genes were critical to the growth of ovarian cancer and not just the JHOC5 cell line, I turned my attention to a recently published public dataset of CRISPR-Cas9 screenings carried out against cell growth and curated by the Broad Institute (Depmap) (Dempster et al., 2019; Meyers et al., 2017). Using an algorithm designed to remove confounding effects from copy number variation (CERES), a dependency score is calculated for each gene in each cell line. These scores are normalized so that a score of 0.0 represents a gene non-essential for growth in a particular cell line, and a score of -1.0 represents a gene highly essential for growth in a particular cell line. I first calculated the differential dependency of each splicing-related candidate gene, representing the relative strength of a given dependency relative to all other screened cell lines, in each ovarian cancer cell line. I next employed a student's t-test to determine which, if any, of these genes have a consistently lower dependency score. The only gene found to be significantly enriched in EOC cell lines versus all other cell lines was the splicing factor DHX38 (Fig. 5). This result was confirmed upon direct comparison of the individual distributions of DHX38 dependency scores by cancer type (Fig. 6A). Further evidence for this trend is provided by plotting the scaled rank of the dependency score of DHX38 as a function of its dependency score across cell lines (Fig. 6B).

It is often the case that gene dependencies in one cancer type are applicable to multiple other cancer types. With this in mind, I analyzed the Depmap screening results

from the lung carcinoma cell line A549, as well as the results from an RNAi screening against the prostate cancer cell line PC3 which have undergone the CERES algorithm (available on the Depmap website), selecting genes with a dependency score of less than -0.2 for further analysis. I also employed my previous JHOC5 screening results, but selected with a less stringent p-value cutoff of 0.2, in order to obtain a similar number of genes to the A549 and PC3 gene lists. The intersection of these three gene lists was then determined, and trimmed using Panther curated gene ontologies (GO:0003824, Catalytic Activity; GO:0098590, Plasma Membrane) to only those genes considered druggable - such as those encoding enzymes, or those which are known extracellular / membrane proteins (Finan et al., 2017; Rask-Andersen et al., 2014). This yielded a list of 92 genes suggested to be critical to the growth of not only ovarian clear cell carcinoma, but lung and prostate carcinoma cells as well. It is of note that DHX38 was present in this final list. I next carried out siRNA-mediated validation experiments on a subset of these genes – DHX38, DDX42, PPP2CA, and DARS. Validation experiments were carried out using three siRNA oligos of differing sequence per gene, used to separately knockdown each candidate gene in each cell line, after which cells were cultured for 4 days and growth monitored via intra-cellular ATP levels (Fig.7). As criteria for growth inhibition, I employed the Cell Titer-Glo assay, which uses intracellular ATP level as a linear indicator of cell number. Validated genes were those whose knockdown resulted in a 40% or greater reduction in growth over the course of the culture period for at least two of the three siRNA oligos. Out of the original four genes assayed, only one, DHX38, was found to be critical for the growth of all three cancer cell lines.

Discussion

While second in prevalence among all ovarian cancer subtypes to the serous subtype, the prevalence of OCCC cases in Asia is nearly 3-times higher than in the west (Anglesio et al., 2011). Clinical treatment of OCCC, especially advanced cases, remains challenging due to the resistance it displays against conventional therapeutic methods. Additionally, the high level of inter-specimen mutational variability seen in OCCC cases without mutations in SWI/SNF complex members or the PIK3CA/ERK/mTOR pathway confounds the development and introduction of precision therapies, whose applicability is often based on the presence of specific sensitizing mutations.

By employing a CRISPR-Cas9 based screening method, I was able to identify eleven novel genes critical to the growth of JHOC5, an OCCC cell line without any of the mutations frequently seen in OCCC. Furthermore, analysis of publicly available CRISPR-Cas9 data sets using OCCC cell lines further implicated DHX38 asbeing critical to OCCC cell growth. Additionally, knockdown of each of the identified candidate genes has been shown to be lethal in cell lines with different tissues-of-origin: the lung carcinoma cell line A549 and the prostate adenocarcinoma cell line PC3 – suggesting that therapies targeting these genes would not only be effective against OCCC but other types of cancer as well. However, in order to confirm the applicability of these genes in the aforementioned cancer types, the effect their knockdown has on growth in normal lung and prostate epithelial cells would need to be determined. DHX38 shows particular promise as it was identified as being critical for the growth of not only the JHOC5 ovarian clear cell carcinoma line where it was first identified, but also for those of the A549 and PC3.

As far as the author is aware, to date, this is thefirst study not only to perform a comprehensive genome-wide CRISPR-Cas9 screening against an OCCC cell line, but also a normal ovarian surface epitheliumcell line in tandem. This distinction is especially important, as the inclusion of a normal sample is critical for the identification of cancer-specific lethalities and growth-promoting mechanisms. Indeed, without the addition of a normal sample, in the present study, an additional 52 genes would have been identified as critical to the growth of JHOC5 cells. Analysis of these genes revealed them to be significantly (FDR < 0.05) enriched with housekeeping genes such as those related to ribosomal assembly (GO:0000027), tRNA metabolism (GO:0006399), and translation (GO:0006412).

In summary, the current CRISPR-Cas9 screening identified three candidate genes as promising therapeutic targets, and further studies/chapters will focus on uncovering the molecular mechanisms by which these genes promote OCCC tumorigenesis and progression.

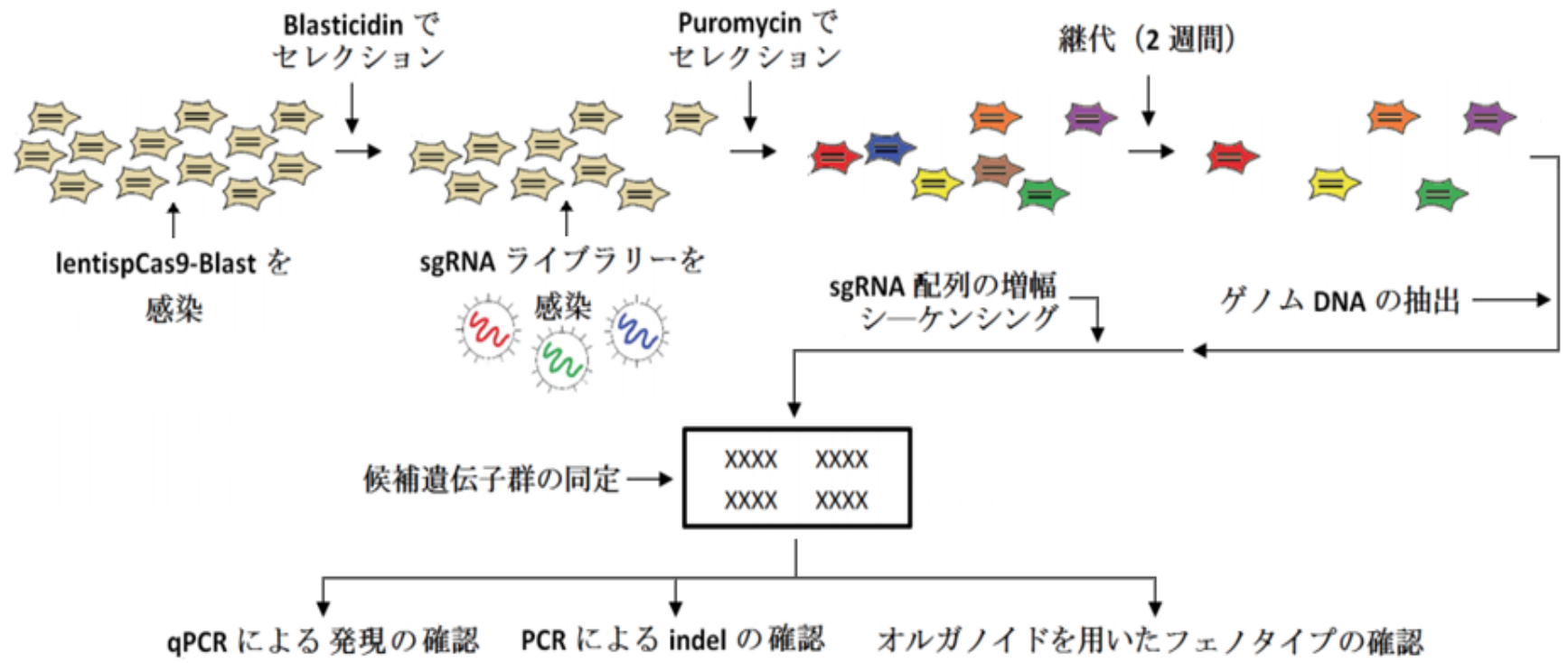

Figure 1. Workflow of the CRISPR-Cas9 screening method. Cells were first infected with a lentivirus containing a Cas9 expression cassette. After selection for stably-expressing cells, cells were infected with a lentivirus containing a comprehensive sgRNA library, and selected for stably-expressing cells. Next, sample was taken as a day 0 time point, and cells were allowed to divide 8 times, after which a second sample of cells was taken. NGS sequencing was then employed to identify the relative sub-populations of each sgRNA, and candidate genes were identified. Finally, candidate genes were validated using RNAi, and functional analyses were carried out.

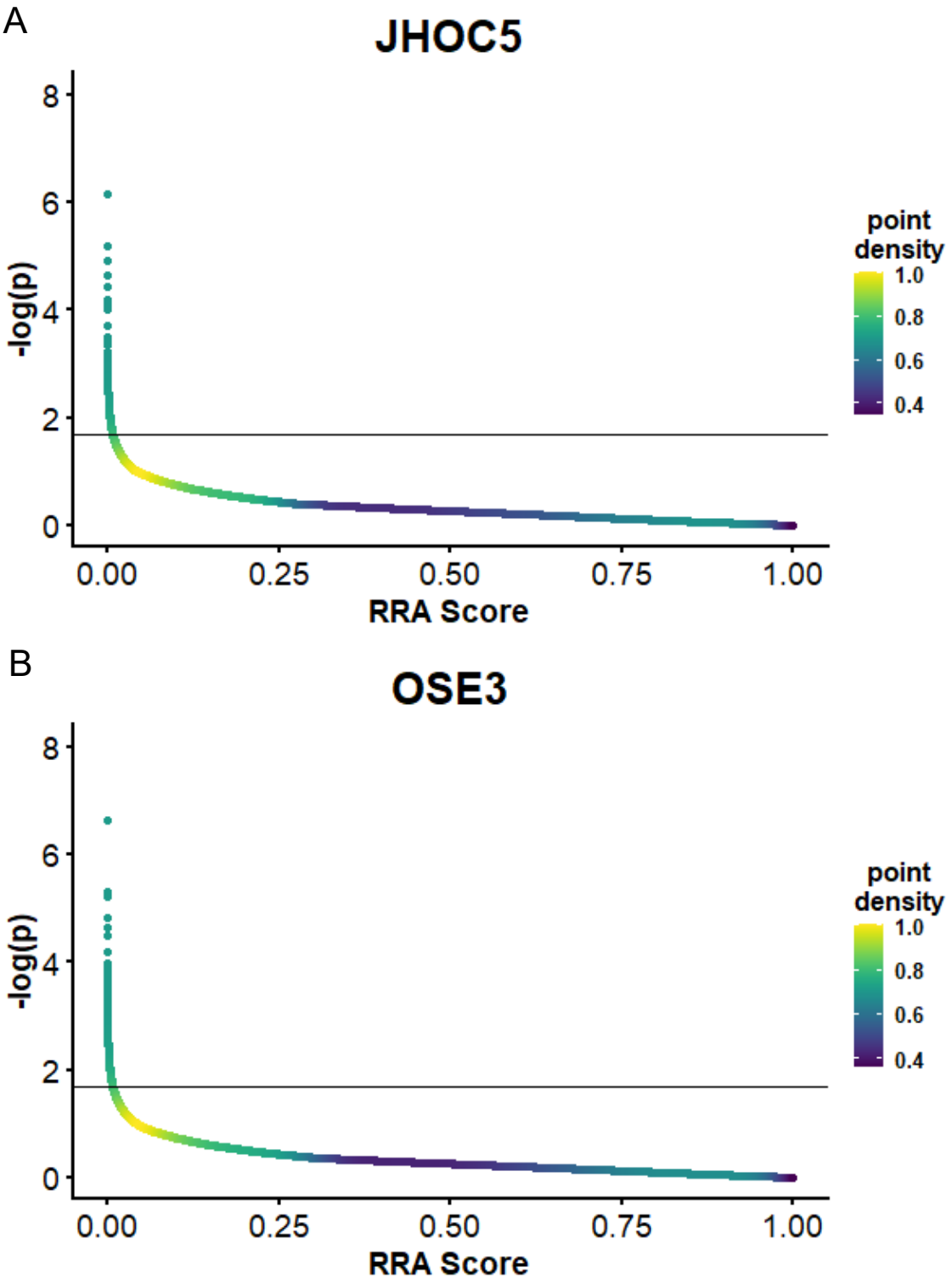

Figure 2. Identification of genes with consistently depleted sgRNAs in (A) JHOC5 and (B) OSE3. Robust Rank Aggregation was used to identify genes whose targeting sgRNAs were most depleted over the course of the culture period. Points represent genes, color indicates density of points (genes), and the dotted line represents p = 0.02.

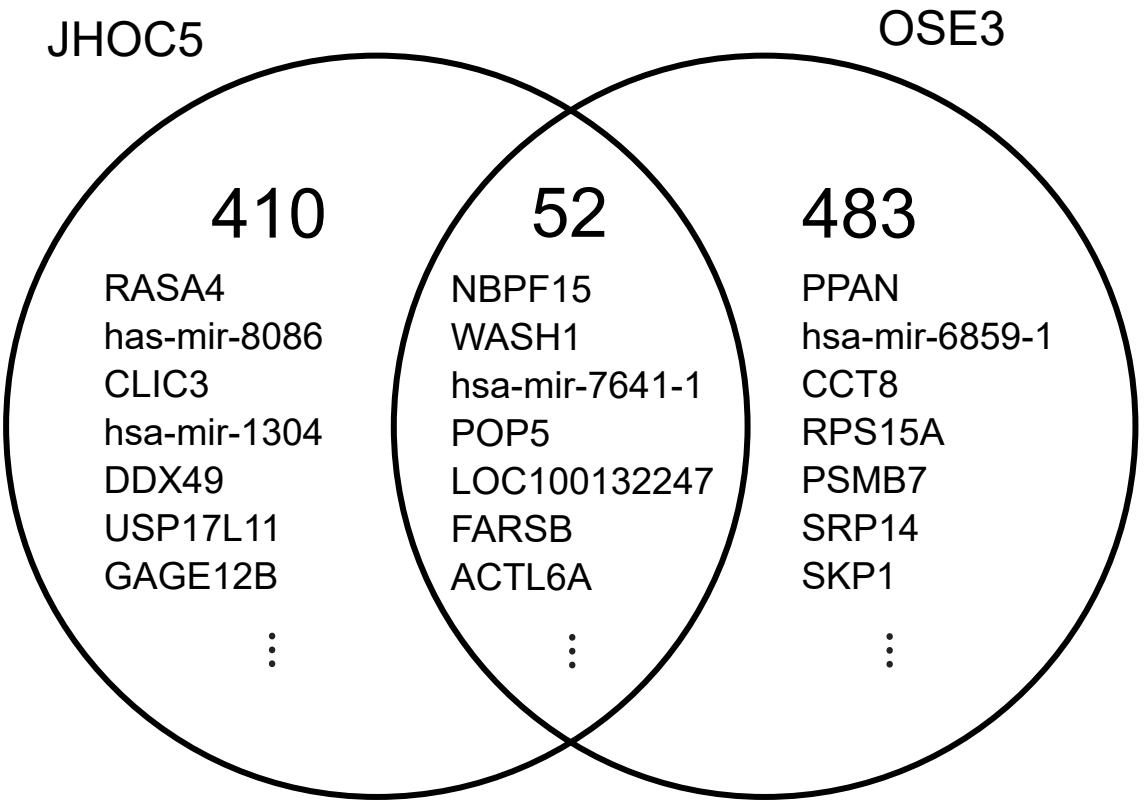

Figure 3. Results of the CRISPR-Cas9 screening against JHOC5 and OSE3. The number of genes identified for each region is displayed, along with the top 7 genes ordered by p-value.

Figure 4. Gene enrichment analysis of JHOC5-specific hit genes. The PANTHER Classification System (reference) was used to assess JHOC5 specific hit genes for statistically overrepresented pathways in the GO-Slim Biological Process ontology set. The top 10 pathways are displayed, along with their associated p-values.

Gene Name	Description
DBR1	Splicing Factor 3A Subunit 3
DHX34	DExH-Box Helicase 34
DHX38	DEAH-Box Helicase 38
DUSP11	Dual Specifity Phosphatase 11
HNRNPL	Heterogeneous Nuclear Ribonucleoprotein L
LSM3	LSM3 U6 Small Nuclear RNA and mRNA Degradation Associated
SAMD4B	Sterile Alpha Motif Domain-Containing 4B
SF3A3	Splicing Factor 3a, Subunit 3
SNRPD3	Small Nuclear Ribonucleoprotein D3 Polypeptide
SRSF3	Serine and Arginine Rich Splicing Factor 3
TRA2A	Transformer 2 Alpha Homolog

Table 1. Gene names and descriptions of splicing-related genes identified in the CRISPR-Cas9 screening against JHOC5 and OSE3.

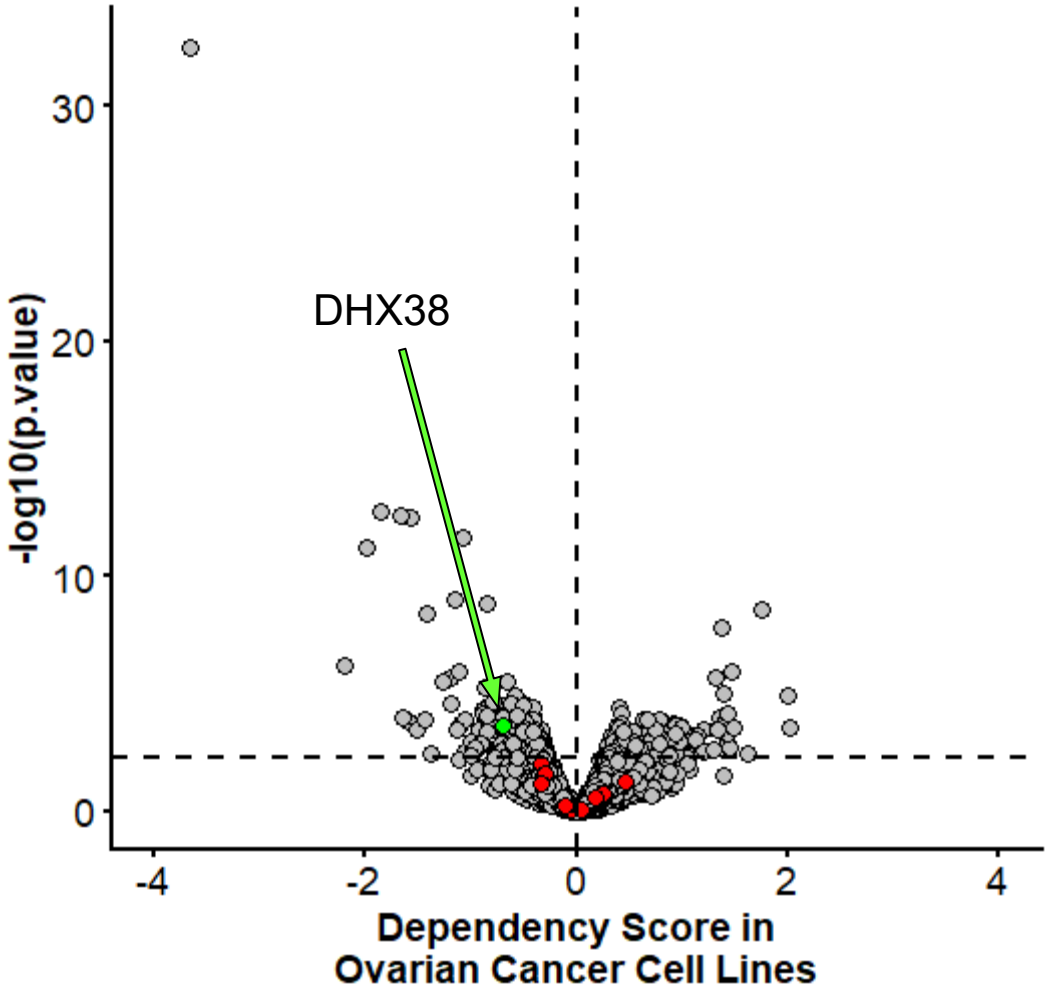

Figure 5. Lineage-specific differential gene dependencies for EOC cell lines. First, the differential dependency of each screening gene in each EOC cell line compared to all cell lines was calculated. The average of this value across EOC cell lines was plotted against an associated p-value, calculated by comparing the differential dependencies of EOC lines versus all other cell lines for each gene using a two-sided student's t-test with unequal variances. Red points represent splicing-related candidate genes identified in the JHOC5/OSE3 screening, green points represent genes from those candidate genes which have an associated p value < 0.0005, and grey points represent all other genes. Horizontal dotted line represents p = 0.0005.

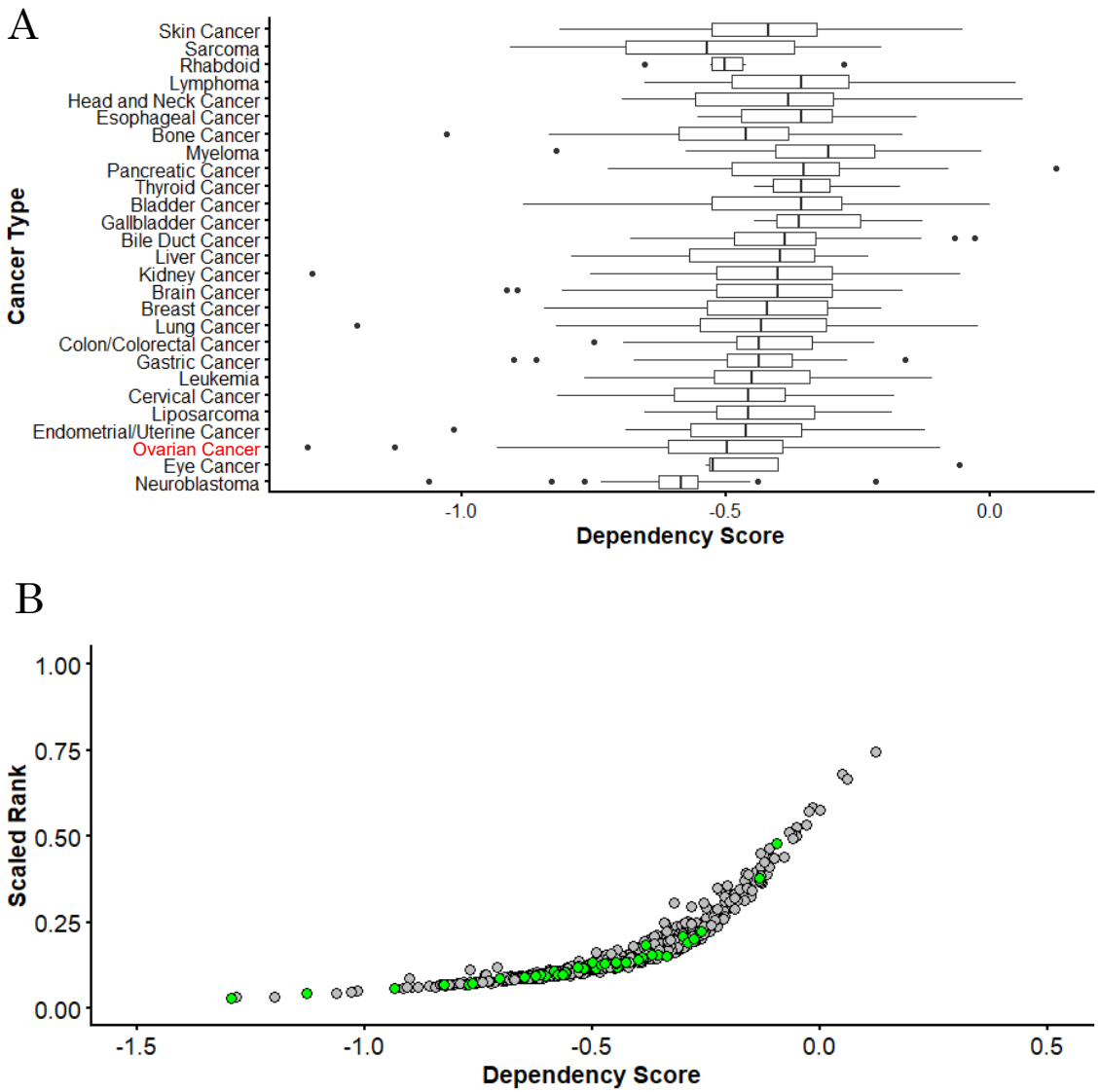

Figure 6. EOC cell lines show a greater dependency on DHX38 than the majority of other cell types. (A) Box plots of dependency scores for cell lines of the designated cancer types. (B) DHX38 dependency scores for all cell lines plotted against the scaled rank of DHX38 across the dependency scores for all genes in that cell line. Grey points represent non-EOC cell lines; green points represent EOC cell lines.

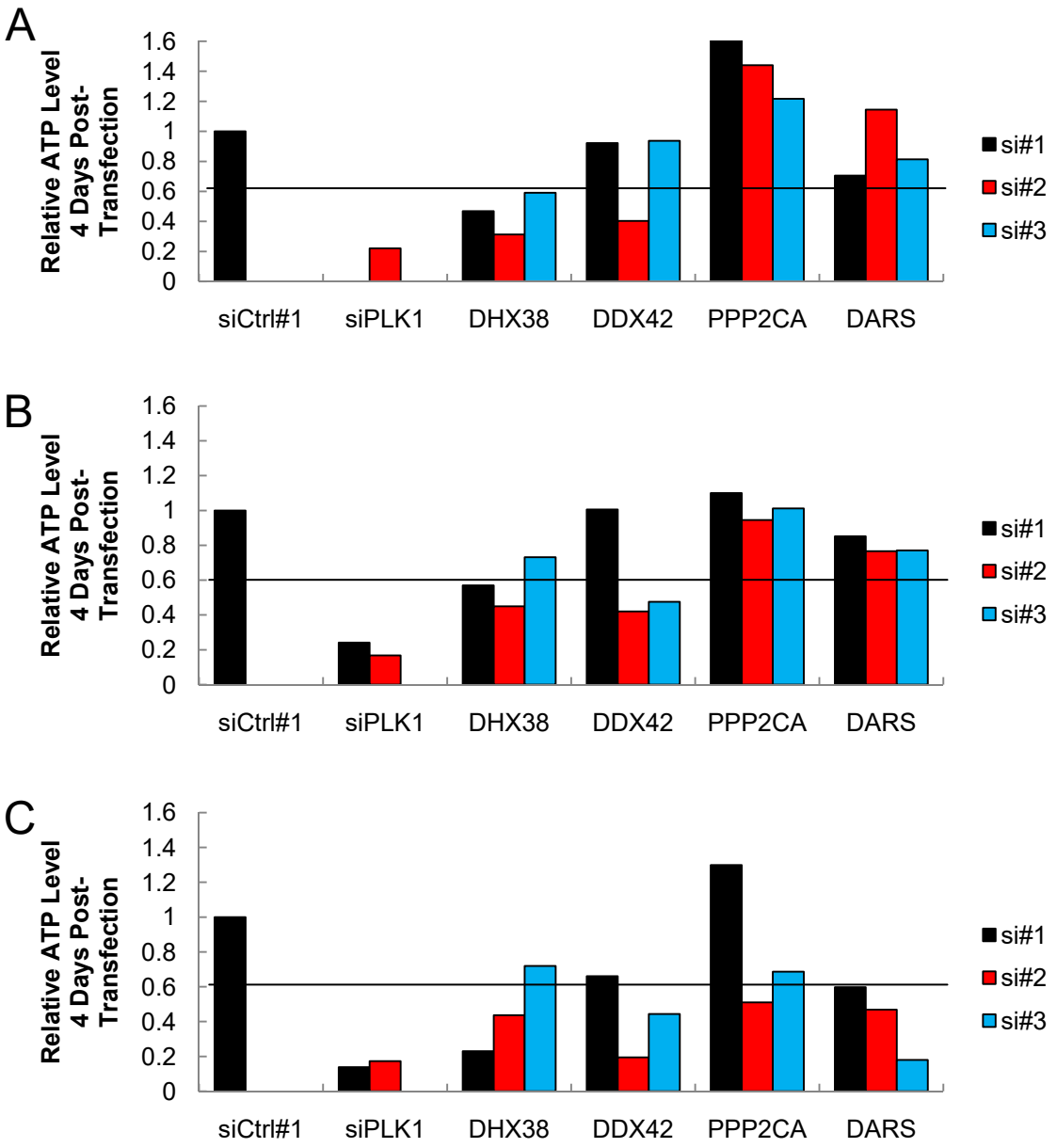

Figure 7. Results of siRNA validation screening against the A) JHOC5 ovarian clear cell carcinoma cell line, B) A549 lung carcinoma cell line, and C) PC3 prostate carcinoma cell line. Cells were transfected with an siRNA targeting the indicated gene upon plating, and intracellular ATP levels were measured on days 1 and 4 via the Cell-Titer GLO kit. Growth data is displayed as the fold change in intracellular ATP level between days 1 and 4, normalized to an siRNA control sequence. Horizontal line represents a relative ATP level of 0.6 compared to a negative control.

Chapter II

DEAH-Box Helicase 38 (DHX38) Functional Analysis

Introduction

In the previous chapter, I carried out a CRISPR-Cas9 growth screen on an OCCC cell line and an OSE cell line, and along with analysis of publically available datasets, uncovered the gene DHX38 as a cancer-specific growth dependency in OCCC. In the current chapter, I carry out functional analysis of DHX38 with the goal of uncovering its role in OCCC tumorigenesis.

DHX38

The DHX38 (DEAH-Box Helicase 38) gene encodes a 150kD RNA-helicase belonging to the DEAH-Box family of proteins, characterized by the presence of the DEAH (Asp-Glu-Ala-His) motif. Missense mutations in DHX38 have been found to correlate with early-onset retinitis pigmentosa, though their role in disease progression has not yet been elucidated (Ajmal et al., 2014; Latif et al., 2018). Additionally, in one study, amplification of DHX38 was found in 56% of acute myeloid leukemia (AML) samples as well as in established AML cell lines (Ma et al., 2006).

The yeast homolog of DHX38, Prp16, has been shown to play essential roles in the yeast spliceosome, specifically in the first splicing reaction, branch point selection, and second splicing reaction (Semlow et al., 2011). A comprehensive analysis of protein-protein interactions of the human spliceosome using yeast two-hybrid experiments has suggested that human DHX38 interacts with proteins involved in the second splicing reaction (Hegele et al., 2012). However, the role that DHX38 plays in the human spliceosome is poorly understood.

DHX38 has also been found to function outside of the spliceosome, where it binds to the PP4 protein phosphatase complex and inhibits the dephosphorylating activity of its PP4C/PP4R2 subunits in both cancer and normal cell lines (Han et al, 2015). However, in OCCC, the function of DHX38 remains uncharacterized.

Apoptosis

One of the hallmarks of tumorigenesis is a tumor cell's acquisition of the ability to evade apoptosis, or programmed cell death. Two major signaling cascades are responsible for the induction of apoptosis: the intrinsic and extrinsic cascades.

One of the major genes responsible for the activation of the intrinsic apoptotic signalingcascade is p53 – known as the 'master regulator' or 'master switch'. This nomenclature is directly due to the diverse number of cellular processes whose dysregulation brings about a highly coordinated response centered on p53, such as DNA damage, oxidative stress, and cell cycle deregulation. Under normal conditions, the p53 protein is kept inactive though its association with Mouse Double Minute 2 Homolog (MDM2), which not only transports it from the nucleus to the cytoplasm to prevent it from acting as a transcription factor, but also acts as a ubiquitin ligase, marking p53 for degradation by the proteosome (Haupt et al., 1997; Michael and Oren, 2003).

However, upon conditions of cellular stress such as DNA damage or prolonged cell cycle arrest, p53 can be stabilized and activated by a wide variety of proteins. For example, upon DNA damage, the kinases ATR and Ataxia telangiectasia mutated (ATM) are known to phosphorylate MDM2 on Ser15 and Ser20, reducing its affinity for p53

(Chehab et al., 1999). Acetylation of MDM2 by CREB-binding protein (CBP)/p300 is also known to stabilize p53 (Ito et al., 2001). Subsequent activation via post-translational modifications then allows p53 to upregulate the transcription of genes responsible for cell cycle arrest and apoptotic induction (Bode and Zigang, 2004).

Another of the major apoptotic signaling pathways, involved in the induction of the extrinsic apoptotic signaling cascade, is the Tumor Necrosis Factor Receptor (TNFR) pathway. TNFR-1 activation through ligand binding leads to the recruitment and activation of TNFR Type 1-Associated DEATH Domain Protein (TRADD) and Fas-Associated Protein with Death Domain (FADD), which subsequently causes caspase-8 to be cleaved and apoptosis to be initiated (Nagata, 1997). An additional effect of TNFR activation is activation of the Nuclear Factor Kappa-Light-Chain-Enhancer of Activated B Cells (NFkB) pathway (Hsu et al., 1995). In the canonical pathway, external activation of TNFRs via ligands such as tumor necrosis factor alpha (TNFα) leads to the activation of IkB kinase (IKK) and subsequently inhibitor of nuclear factor kappa B (IkB) phosphorylation, ubiquitination, and degradation (Karin, 1999). Converted from a trimer to a dimer by the degradation of IkB, the remaining NFkB complex (consisting of a dimer of Transcription Factor p65 (RelA) and NFkB p105 Subunit (NFKB1)) then translocates to the nucleus, where it is known to regulate the transcription of a number of genes responsible for cell growth, proliferation, and apoptosis, depending on cell type (Kühnel et al., 2000; Sun et al. 2010). In the non-canonical pathway, activation of NIK followed by phosphorylation of IKKα leads to phosphorylation of p100, which is subsequently cleaved into p52, and is translocated to the nucleus along with RelB, to regulate the transcriptional activity of RelA as well as the transcription of a number of genes, including pro-apoptotic factors

(Li et al., 2011; Matos and Jordan, 2006).

One of the major subsets of genes showing increased transcription upon p53 / NFkB activation is the Bcl-2 family of mitochondrial membranepermeabilizers (Kale et al., 2018). This family of proteins is divided into three subfamilies; the anti-apoptotic (Bcl-2, Bcl-W, Bcl-X_L, MCL-1, etc.), the BH3-only pro-apoptotic (Bad, Bid, Bik, Bim, Bmf, NOXA, PUMA, etc.), and the pore-forming executioner pro-apoptotic (Bax, Bak, Bok) proteins. These proteins are localized to the outer mitochondrial membrane, where the relative levels of pro- and anti- apoptotic members, all binding to one another via their shared BH3 domain, results in the formation of a Bax/Bak homo-oligomer upon their binding to the pro-apoptotic family members. Homo-oligomers of the pore-forming Bcl-2 subfamily members act as pores through which cytochrome C can exit the mitochondria and initiate apoptosis. Many pro-apoptotic BH3-only members of the Bcl-2 family are directly upregulated transcriptionally through the action of p53, such as NADPH oxidase activator 1 (NOXA), p53 upregulated modulator of apoptosis (PUMA), and Bax, and it has been shown that p53 both transcriptionally represses and directly binds to and deactivates the anti-apoptotic BCL-2 gene (Hemann and Lowe, 2006).

Splicing and Apoptosis

Alternative splicing has been shown to play a role in the induction of apoptosis. Proofreading of splice sites during the first and second splicing reactions by the multitude of splicing factors present allows the splicing machinery to select alternative splice sites. This results in numerous possible mRNA variants per coding gene, with

some studies estimating that over 70% of human genes undergo alternative splicing (Johnson et al., 2003). In certain cases, promotion of certain variants over others can have either an apoptosis-promoting or inhibitory effects. A classic example of this is the BCL-X gene, a member of the Bcl-2 family of mitochondrial membrane permeabilizers. BCL-X can be alternatively spliced into one of two possible variants based on the phosphorylation status of the Sam68 splicing factor (Paronetto et al., 2007). The long form, Bcl-X_L, binds to and competitively deactivates other pro-apoptotic Bcl-2 family members (Billen et al., 2008). The shorter variant Bcl-X_S has been found to bind to and inhibit the anti-apoptotic Bcl-2 family members Bcl-X_L and Bcl-2, allowing pro-apoptotic family members to be released and promote apoptosis (Lindenboim et al., 2001). Modulation of splicing factor activity is not the only mechanism by which cancer cells promote alternative splicing of tumorigenic variants. For example, hotspot mutations in the SRSF2 gene alter its preference of RNA binding sites which result in the altered splicing of multiple mRNAs (Pangallo et al., 2020). Additionally, in MYC-transformed cells, the MYC gene has been found to specifically upregulate certain splicing factors such as SRSF1, which results in various tumor-promoting effects through the induction of alternative splicing such as the promotion of long-form RAF expression and the upregulation of an oncogenic form of the S6K1 gene, leading to increased phosphorylation of 4E-BP1 and more efficient cap-dependent translation (Ben-Hur et al., 2013; Das et al., 2012; Hsu et al., 2015; Rauch et al., 2011)..

Materials and Methods

Cell Culture

JHOC5 ovarian clear cell carcinoma cells as well as OSE1 and OSE3 normal ovarian surface epithelium cells were cultured in RPMI1640 medium supplemented with 10% fetal bovine serum (FBS) and 2 mM L-glutamine. HEK293FT human embryonic kidney cellsand OVISE ovarian clear cell carcinoma cells were cultured in DMEM medium supplemented with 10% FBS and 4 mM L-glutamine. ES2 ovarian clear cell carcinoma cells were cultured in McCoy's 5A Medium supplemented with 10% FBS. TOV21G ovarian clear cell carcinoma cells were cultured with a 1:1 mixture of MCDB 105 medium and Medium 199, supplemented with 15% FBS and 1.85 g/L sodium bicarbonate. All cell lines were cultured at 37°C under a 5% CO_2 atmosphere.

shRNA Lentiviral Preparation, Infection, and Transplant

shRNA vectors (shLuc-GATTTCGAGTCGTCTTAAATGT, shDHX38#1 - GAAGGAATTTCATTTGACACG, shDHX38#2 - GATCACATGAAGAGAAAGAGC) were inserted into the CS-Rfa-CG backbone. Lentiviruses were prepared via co-transfection of HEK293FT cells with the appropriate vector along with the packaging plasmids psPAX2 and pMD2.G using polyethylenimine 'MAX' (PEI, Polyscience, Inc. Cat. 24765) in a 4:6 mix of OPTIMEM:DMEM, and collected via ultra centrifugation after 72 hours. Viral titers were determined using TOV21G cells. For shRNA experiments, JHOC5 cells were infected at an MOI of 25, OSE1, TOV21G, and ES2 cells were infected at an MOI of 50, and OSE3 cells were infected at an MOI of 100. For transplantation of TOV21G cells, 1.5 x 10^6 infected cells were injected into

the flanks of Balb/c nu/nu mice and tumor volume was measured periodically.

siRNA transfection

Adherent cells were trypsinized and dissociated from plates. Lipofectamine RNAiMAX Transfection Reagent (Invitrogen) was diluted in Opti-MEM I reduced serum medium (Opti-MEM) such that it would have a final concentration in the transfection medium of 1% v/v, and allowed to equilibrate briefly. Separately, siRNA oligomers purchased from Ambion (siCtrl#1 - #4390844, siDHX38#1 - s18906, siDHX38#2 - s18908) were diluted in Opti-MEM such that their final concentration in the transfection medium was 10 nM. The equilibrated RNAiMAX solution and an equal volume of diluted siRNA solution were mixed, vortexed, and allowed to incubate at room temperature for 20 minutes. At the end of the incubation period, an appropriate volume (1 part) of transfection medium was added per well, followed by an appropriate volume (5 parts) and density of dissociated cells.

Growth Assays

Cell growth was assayed using the Cell-Titer Glo Luminescent Cell Viability Assay (Promega). After removing culture medium, cells were washed once with PBS, and an appropriate amount of Cell-Titer Glo Reagant diluted 4x in PBS was added. Plates were then shaken at room temperature for 10 minutes, after which fluorescence was measured using a Mithras LB 940 Plate Reader (BERTHOLD).

Protein Extraction and Western Blot

Cells were harvested and lysed using 1% NP-40 buffer (50 mM Tris-HCl, 0.14 mM NaCl, 1 mM EDTA, 1% NP-40) along with 1x Halt Protease Inhibitor Cocktail (Thermo Scientific). Protein concentration was measured using the BCA assay as described by the manufacturer. Proteins were separated by SDS-PAGE and transferred to an Immobilion PVDF Membrane by electroblotting. After membranes had been blocked with skim milk, and incubated with primary and secondary antibodies (DHX38 – 10098-2-AP (proteintech), GAPDH – MAB374 (Millipore), p53 DO-1 – (Santa Cruz), HRP-linked ECL Sheep anti-Mouse IgG (GE), HRP-linked ECL Donkey anti-Rabbit IgG (GE)), protein bands were visualized using HRP substrate (Millipore) and a BIO-RAD ChemiDoc Imaging System.

RNA extraction and Reverse Transcription

Total RNA was extracted from cells and purified using TRIsure (BIOLINE) following the manufacturer's protocol, using 1mL of reagent per 1 x 10^6 cells. RNA pellets were resuspended in MilliQ and stored at -80°C. Synthesis of cDNA was carried out using Prime Script RT Master Mix (TaKaRa).

qRT-PCR

Synthesized cDNA was mixed with an appropriate volume of primers and 2x SYBR Green Master Mix (Applied Biosystems), and measured on a LightCycler480 (Roche). The ΔΔCT method was used to quantify concentrations relatively, with GAPDH being used as an internal control.

RT-qPCR primers are as shown below.

GAPDH forward: GCACCGTCAAGGCTGAGAAC

GAPDH reverse: TGGTGAAGACGCCAGTGGA

DHX38 forward: GCGGGATAGAAGTAGGCACAG

DHX38 reverse: GAAGGGGTGGCTGCATCTTTA

p53 forward: AGGCCTTGGAACTCAAGGAT

p53 reverse: CCCTTTTTGGACTTCAGGTG

PUMA forward: GACCTCAACGCACAGTACGA

PUMA reverse: AGGACCCTCCAGGGTGAG

GADD45A forward: GCCAAGCTGCTCAACGTC

GADD45A reverse: CTCTGTCGTCGTCCTCGTC

BCL2 forward: AGTACCTGAACCGGCACCTG

BCL2 reverse: GGGCCGTACAGTTCCACAAA

AnnexinV-FITC / PI Apoptosis Assay

Annexin V-FITC / PI Apoptosis Assays were carried out using the MEBCYTO-Apoptosis Kit (MBL) following the manufacturer's instructions.

Sub-G1 Assays

Cells infected with shRNA-containing lentiviruses and cultured for either 4 or 5 days. Cells were then trypsinized, collected, and fixed in a 70% ethanol:water solution at -30°C overnight. The following day, cells were incubated in a 4 mM citric acid (pH 8.0), 200 mM (Na_2HPO_4) solution for 20 minutes, after which they were stained with asolution of 10 μg/mL propidium iodide and 10 μg/mL RNase A in 1x PBS for an

additional 20 minutes and analyzed on a Sony EC800 Flow Cytometry Analyzer.

Next-Generation RNA-seq

Total RNA was isolated with TRIsure reagent (BIOLINE). RNA-seq libraries were constructed using the TruSeq RNA Sample Prep Kit and sequenced in the 150bp pair-end reads on a HiseqX platform (Illumina) at Annoroad Gene Technology. Sequenced paired-end reads were aligned onto a reference genome (GRCh38/hg38) using STAR 2.5.3a (Dobin A et al., 2013) and then quantified expression levels of genes and transcripts with RSEM 1.3.1 (Li B et al., 2011). Qualimap (García-Alcalde F et al., 2012) was used for estimating coverage across the reference.

Data and Statistical Analyses

Statistical analyses, including students' t-tests, were performed using R version 3.6.0 (http://www.r-project.org/). RNA-seq data was analyzed using the EdgeR package (McCarthy et al., 2012; Robinson et al., 2010). GSEA analyses were performed using the Msigdbr package (Liberzon et al., 2015; Tamayo et al., 2005). Transcription factor enrichment analysis was performed using the ChEA3 tool (Keenan et al., 2019).

Results

The CRISPR-Cas9 screen carried out in chapter I demonstrated that DHX38 expression is critical for the growth of the OCCC cell line JHOC5. To ensure that this growth dependency was not JHOC5-specific, I first employed siRNA to knockdown DHX38 expression in a plethora of OCCC cell lines with various mutational signatures (Table 2) as well as two T-antigen immortalized OSE cell lines (OSE1, OSE3), and monitored their growth using the Cell-Titer Glo intracellular ATP assay. I found that knockdown of DHX38 induces a significantly larger reduction in growth in three (JHOC5, TOV21G, ES2) OCCC cell lines compared to two (OSE1, OSE3) OSE cell lines after four days of culture (Fig. 8A,B). I additionally found that extended culture (7 days) of the TOV21G cell line resulted in a short initial period of growth followed by a sharp decrease in cell viability, to the extent that cell numbers 7 days post-transfection are implied to be of similar numbers to those 1 day post-transfection (Fig. 8C). Knockdown of DHX38 via shRNA in several OCCC cell lines followed by extended culture (7 days) allowed me to confirm this trend (Fig. 9A); namely that prolonged knockdown (Fig. 9B,C) of DHX38 in OSE cells did not result in the same decrease in growth seen in OCCC cells. To confirm whether this decrease in growth could be replicated in vivo, I established three TOV21G cell lines each constitutively expressing either one of two shRNAs targeted to DHX38 or to the luciferase gene and implanted them into the flanks of immunocompromised mice (Fig. 10). Mice implanted with TOV21G cells infected with a control shRNA expression cassette against the luciferase gene all began developing tumors after 4 weeks, whereas mice implanted with shDHX38-expressing cells did not begin to develop tumors until 4 weeks. Additionally,

the average tumor mass of the shLuc cohort was found to be significantly ($p < 0.005$) less than either of the two shDHX38 cohorts. These results provide evidence that DHX38 expression is critical for the growth of OCCC cells, but not for that of OSE cells.

I next turned my attention to the sharp decrease in cell viability seen between 4 and 7 days post-transfection with an siRNA targeting DHX38 in TOV21G cells. One possibility is that this decrease can be attributed to an increase of cell death resulting from a lack of DHX38, as approaching day 7, adherent cell numbers were seen to decrease dramatically with a concomitant increase in non-viable non-adherent cells (Data not shown). I first determined the effect of sh-mediated DHX38 knockdown in OSE1, OSE3, JHOC5, and OVISE cells on apoptosis using flow cytometry after staining with propidium iodide (Fig. 11). Treatment with an shRNA targeting DHX38 resulted in an increase in the number of Sub G1 events occurring in OCCC cells compared to a cohort expressing shLuc, but not in OSE cells. I next performed an AnnexinV-FITC / PI apoptosis assay on TOV21G cells four days post-transfection with one of two siRNAs targeting DHX38 (Fig. 12). I was able to confirm a nearly three-fold increase in apoptotic cells at this time point. Additionally, I determined the effect of DHX38 knockdown on the expression of several pro- and anti-apoptotic genes in OSE1, OSE3, TOV21G, ES2, JHOC5, and OVISE cells via qPCR. I found that DHX38 knockdown results in a cancer-specific upregulation of both PUMA, a potent pro-apoptotic factor, as well as GADD45A, which aside from its role in cell cycle arrest has also been shown to play a role in the induction of apoptosis (Fig. 13). I also discovered that upon knockdown of DHX38 in OSE1 and OSE3 cells, there was a notable increase in the expression of the anti-apoptotic BCL2 gene. Interestingly, even

though the ES2 OCCC cell line harbors a mutation in one allele of p53, it still shows a level of growth inhibition upon DHX38 knockout similar to p53 non-mutant OCCC lines. Taken together, these data show that DHX38 knockdown results in an OCCC-specific induction of apoptosis, and that this induction occurs irrespective of p53 mutation status. The yeast homolog of DHX38, Prp16, is known to play a critical role in the yeast spliceosome; additionally DHX38 is known to associate with the human spliceosome. Aberrations in the splicing machinery are known to play a role in both the promotion and inhibition of apoptosis, as well as in the modulation of the transcriptome as a whole. In order to provide insight into the role DHX38 plays in the OCCC transcriptome, I carried out RNA-seq analyses on OSE3, TOV21G, and ES2 samples transfected with either a control siRNA or one of two siRNAs against DHX38. The EdgeR package was used to identify genes differentially expressed in control samples vs. DHX38-knockdown samples (Fig. 14A-C). The full list of fold changes for each gene was analyzed using GSEA (Gene Set Enrichment Analysis), and pathways differentially expressed at an FDR of 0.05 or less were determined (Fig. 14D-F). Of these pathways, the TNFα/NFkB pathway was found to be significantly activated in both ES2 and TOV21G cells upon DHX38 knockdown, but not in OSE3 cells (Fig. 14D-F, Fig. 15). Analysis of transcription factors with binding sites upstream of the core genes identified in both TOV21G and ES2 (Fig. 16A) in this pathway using ChEA3 (Keenan et al., 2019) identified a number of candidate transcription factors controlling the transcription of these genes, including both RelB and NFKB2, the two members of the NFkB family which comprise the non-canonical NFkB pathway (Fig. 16B).

Additionally, many pathways involved in the regulation of the cell cycle, such as the G2/M checkpoint, targets of the E2F transcription factor which are essential for

DNA replication and G1/S transition, and components of the mitotic spindle were downregulated in an OCCC-specific manner. Analysis of sequencing reads uncovered that knockdown of DHX38 increases the percentage of reads that contain intronic sequences, but the percentage of reads containing overlapping exonic and intronic or intergenic sequences was relatively constant (Fig. 17).

Discussion

In the present study, it was discovered that knockdown of DHX38 in OCCC cell lines, but not in OSE cell lines, resulted in inhibition of cell growth, and that this inhibition is at least in part due to the induction of apoptosis in an OCCC cell-specific manner. It is also of note that in OSE cells, knockdown of DHX38 resulted in the transcriptional upregulation of BCL2, an anti-apoptotic protein (Fig. 17). While the presence of the large T antigen in OSE1 and OSE3 could possibly be acting to attenuate the same pro-apoptotic signals present after DHX38 knockdown in OCCC cells through the inactivation of p53, this fact is insufficient to explain why BCL2 expression is upregulated in this manner. Elucidation of the signaling pathways upstream of BCL2 in OSE cells may give clues to the cause of this phenomenon, and will be important to make clear the applicability of the results of the present study to the ovarian surface epithelium. Furthermore, of the OCCC cell lines screened, one (ES2) has a deactivating mutation in one allele of p53. While this would suggest that ES2 may be less susceptible to DHX38 knockdown mediated growth inhibition (Fig. 12, 13A and 13B) were it to be mediated by a p53-coordinated response, no such attenuation of growth inhibition was seen. This is strong evidence against the involvement of p53 in DHX38 knockdown-mediated apoptosis.

RNAi-mediated knockdown of DHX38 expression was previously discovered to inhibit the growth of colorectal carcinoma cells in a KRAS mutation state-dependent manner (Fraile et al., 2017). However, of the three OCCC cell lines employed in the current study, only one (TOV21G) has an activating mutation in KRAS or the pathways canonically downstream of KRAS. This would suggest that while DHX38 growth

dependency in colorectal cancer cells may rely on the activity of KRAS, the link between the two in OCCC may not be as strong.

RNA-seq of DHX38-knockdown and control OCCC and OSE cell lines showed that DHX38 knockdown leads to a slight increase in intronic reads, but not in reads containing exon / intron boundaries. This could be a result of a higher percentage of transcripts being immature, due to a retardation of the splicing machinery. It may also be a result of previously uncharacterized splicing events. However, significant identification of splicing event changes / aberrations is not feasible with the number of replicates and at the read depth used in the current study. Further studies may be warranted at higher read depths in order to determine the effect DHX38 knockdown has on alternative splicing in OCCC. Additionally, RNA-seq results uncovered a significant increase in the expression of several major inhibitory members of the canonical NFkB (p50/p65) pathway in OCCC cell lines, but not in OSE cell lines. Specifically, direct inhibitors of p50/p65 complex transcription and activation, such as TNFAIP3, ETS2, NFKBIA, NFKBIE, KLF2, RCAN1, and TNIP1, were shown to be upregulated in a cancer-specific manner (Das et al., 2018; Jacobs and Harrison, 1998; Jha and Das, 2017; Oshima 2017; Whiteside et al., 1997; Chen et al., 2017). Interestingly, however, several targets of NFkB signaling involved in the negative regulation of cell growth and the cell cycle (DRAM1, GADD45A, LAMB3, PER1, ICAM1, and ZC3H12A) as well as positive regulation of apoptosis (CXCL2, LAMB3) were also found to be upregulated in the OCCC cell lines (Chen et al., 2001 ; Chen et al., 2019 ; De Plaen et al., 2006 ; Ding et al., 2018 ; Kasza et al., 2010 ; Lu et al., 2019 ; Reina et al., 2017 ; Stanisavljevic et al., 2012 ; Suzuki et al., 2008 ; Van der Vaart et al. 2014 ; Zhang et al., 2019), several of which also act as negative regulators of NFkB. This may be due to non-canonical NFkB

signaling (via RelB and/or c-Rel). Crosstalk between p65-containing NFkB complexes and those containing RelB have been identified; several genes shown to be upregulated upon DHX38 knockdown in the present study (DRAM1, CSF1, CXCL2, and CXCL3) have already been identified as RelB target genes (Chanut et al., 2014; Waters et al., 2019). Indeed, analysis of the profile of the transcription factors which bind to the core enrichment genes identified via GSEA (Fig. 19 and 20B) identified RelB as the most significantly enriched. Additionally, the canonical p65 has been shown to have a pro-tumorigenic effect in OCCC, transcriptionally activating genes coding for inflammatory cytokines to promote growth (Kim et al., 2016). However, the role of non-canonical NFkB signaling, including that of RelB, in OCCC has yet to be elucidated, and may be the subject of future work.

Cell Line	Mutations
JHOC5	
OVISE	PIK3CA, ARID1A, ARID1B, PPP2R1A, STAT3
ES-2	TP53, BRAF, JAK1
TOV21G	PIK3CA,ARID1A, ARID1B, KRAS, PTEN, CTNNB1, JAK1

Table 2. OCCC cell lines used in RNAi screening of DHX38. CCLE was used to identify mutations common to OCCC (ARID1A, ARID1B, SMARCA4, PIK3CA, PTEN, TP53, KRAS, BRAF, CTNNB1, TERT, PP2R1A, JAK, STAT3) in each cell line.

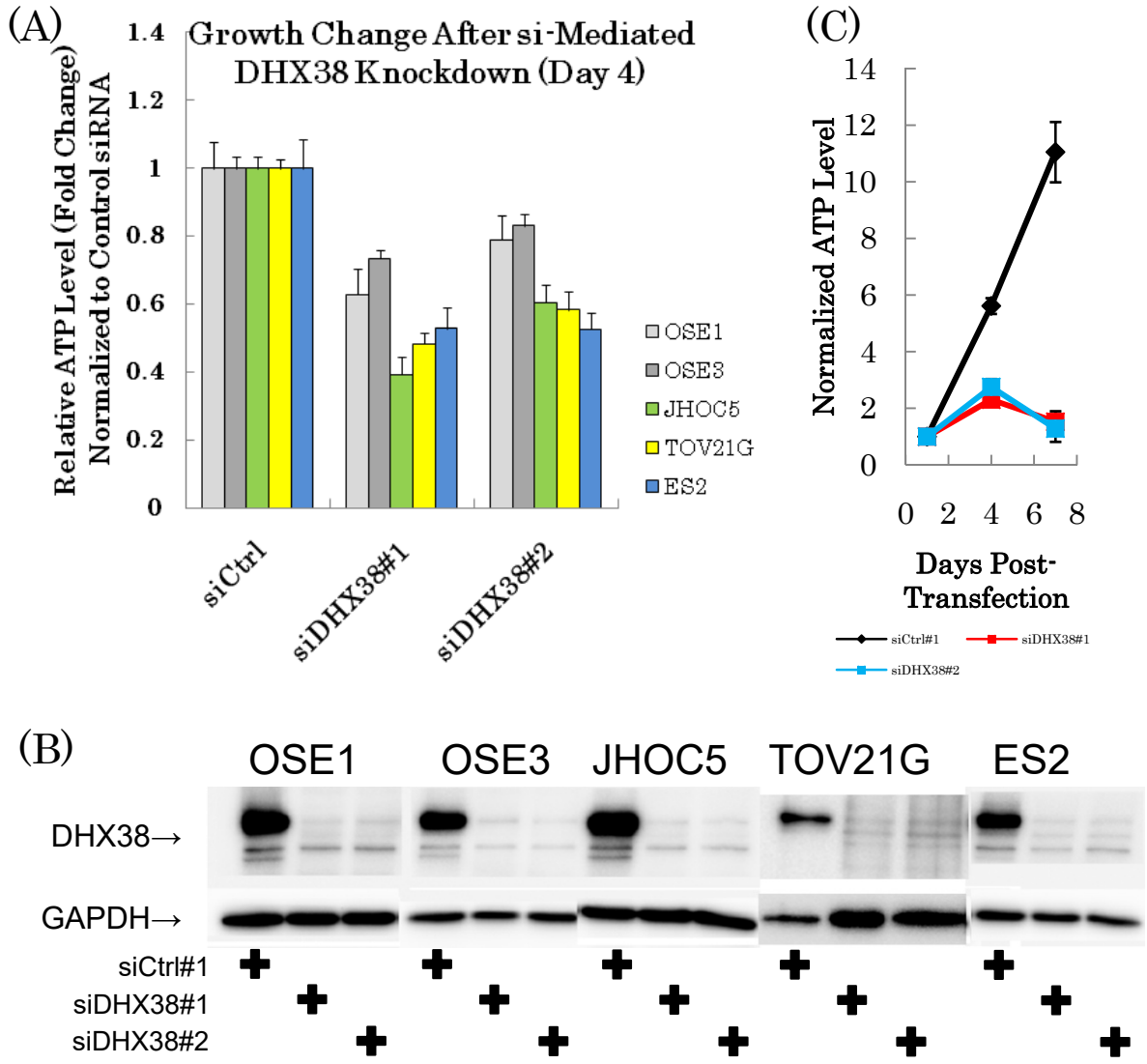

Figure 8. siRNA-mediated knockdown of DHX38 induces cancer-specific growth inhibition. (A) Fold change of intercellular ATP level as a measure of cell growth in OSE cell lines (gray) and OCCC cell lines (colored) 4 days post-transfection with a control siRNA or an siRNA targeting DHX38. (B) Protein levels of Gapdh (internal control, bottom) and Dhx38 (top) upon transfection with a control siRNA or an siRNA targeting DHX38.(C) Intercellular ATP level time-course of TOV21G cells treated with siDHX38, normalized to 1 day post-transfection.

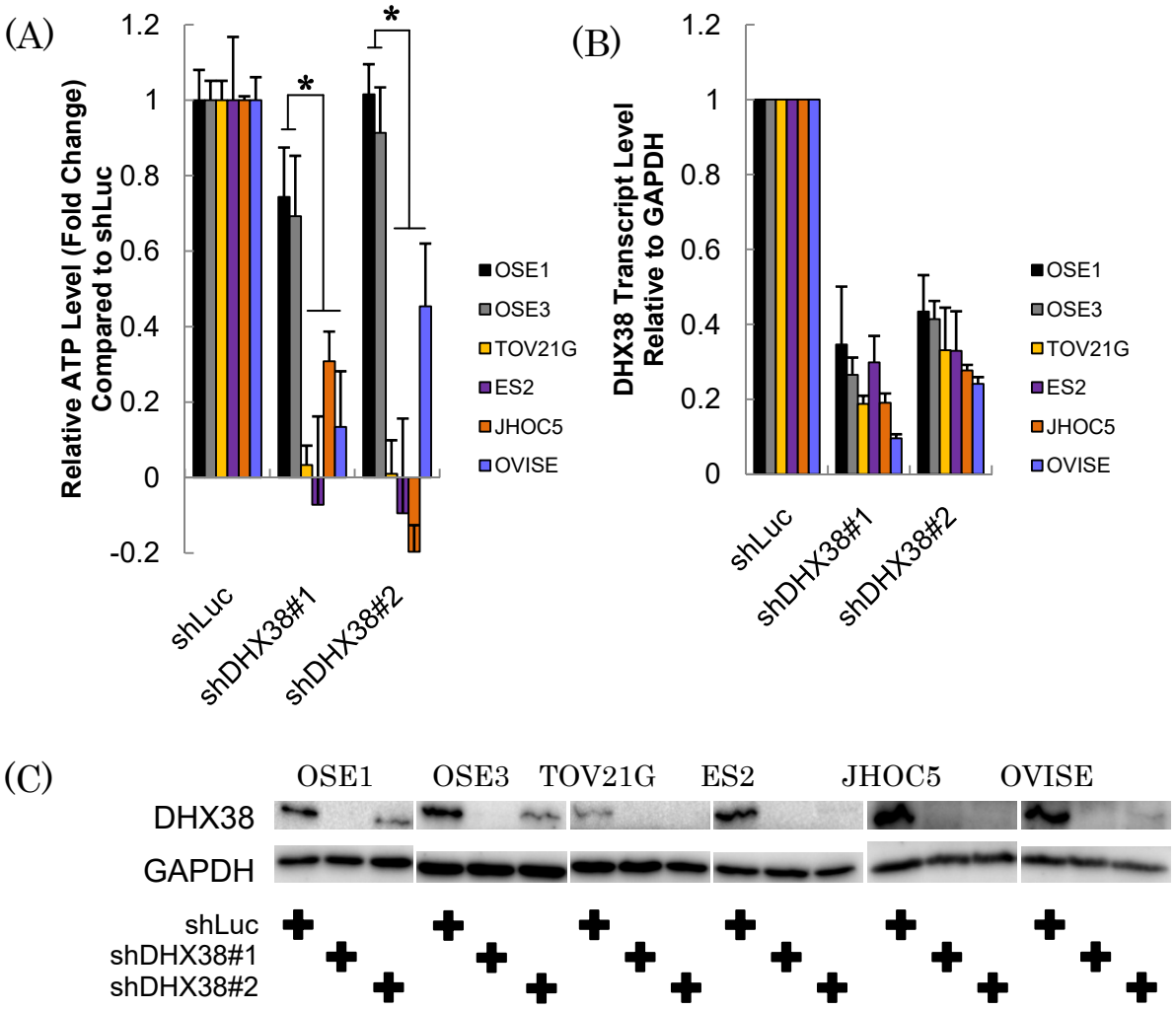

Figure9. shRNA-mediated knockdown of DHX38 in OSE and OCCC cell lines leads to an OCCC-specific inhibition of cell growth. (A) Intracellular ATP level was measured in the indicated cell lines 1 day and 7 days post infection with shRNA-containing lentiviruses. Data is displayed as the log2 of the ratio between ATP level on days 1 and 7, normalized to shLuc (*, $p < 0.05$; individual unpaired t-test; unequal variances; all data $n \geq 3$). (B)Knockdown efficiencies were determined for the given shRNAs in the given cell lines 4 days post infection. Data is expressed as transcript level relative to GAPDH, normalized to shLuc. (C) Protein expression levels of DHX38 (upper) and GAPDH (lower) were determined via western blot for shDHX38.

(A)

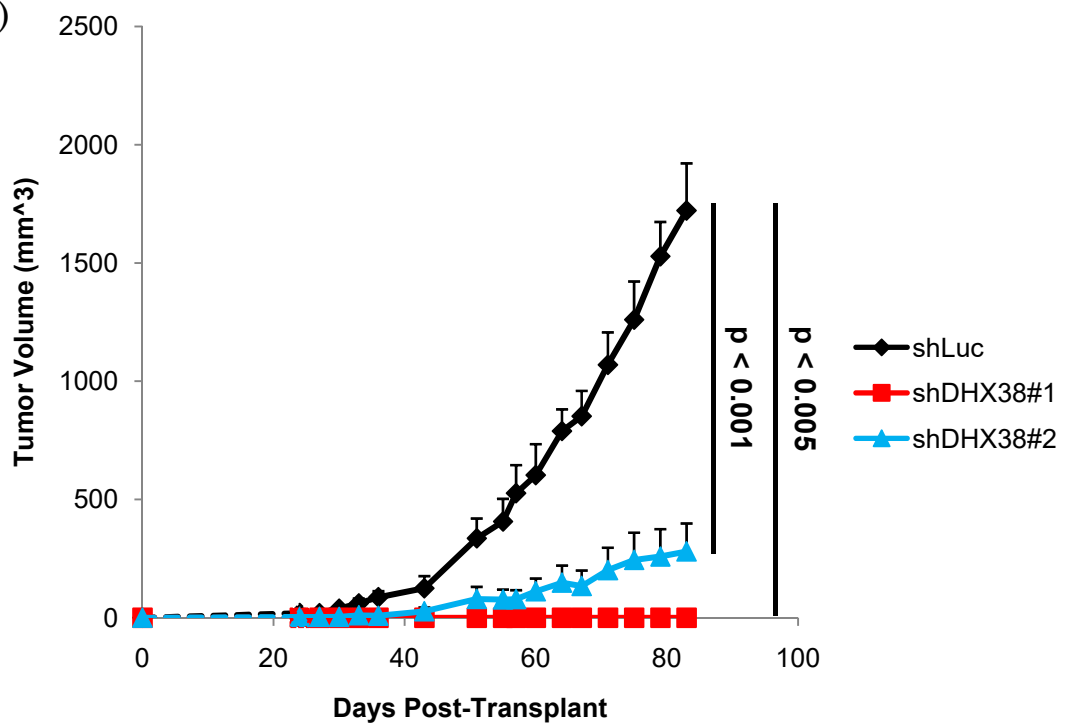
2500
2000
1500
1000
500
0
Tumor Volume (mm^3)
0
20
40
60
80
100
Days Post-Transplant
p < 0.001
p < 0.005
shLuc
shDHX38#1
shDHX38#2

(B)

(C)

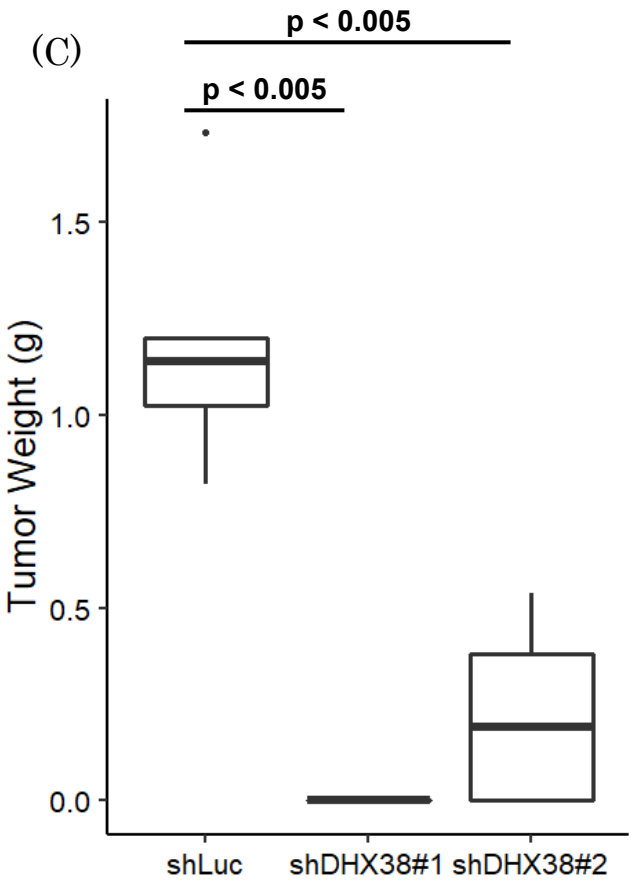
p < 0.005
p < 0.005
1.5
1.0
0.5
0.0
Tumor Weight (g)
shLuc
shDHX38#1
shDHX38#2

Figure 10. DHX38 knockdown impairs TOV21G tumor formation ability. (A) Tumor volume of mice subcutaneously injected with TOV21G cells expressing either shLuc or one of two shRNAs against DHX38 (n = 5; unpaired student's t test). (B) 83 days post-transplantation, tumors were removed, sectioned, and (C) weighed (n = 5; unpaired student's t test).

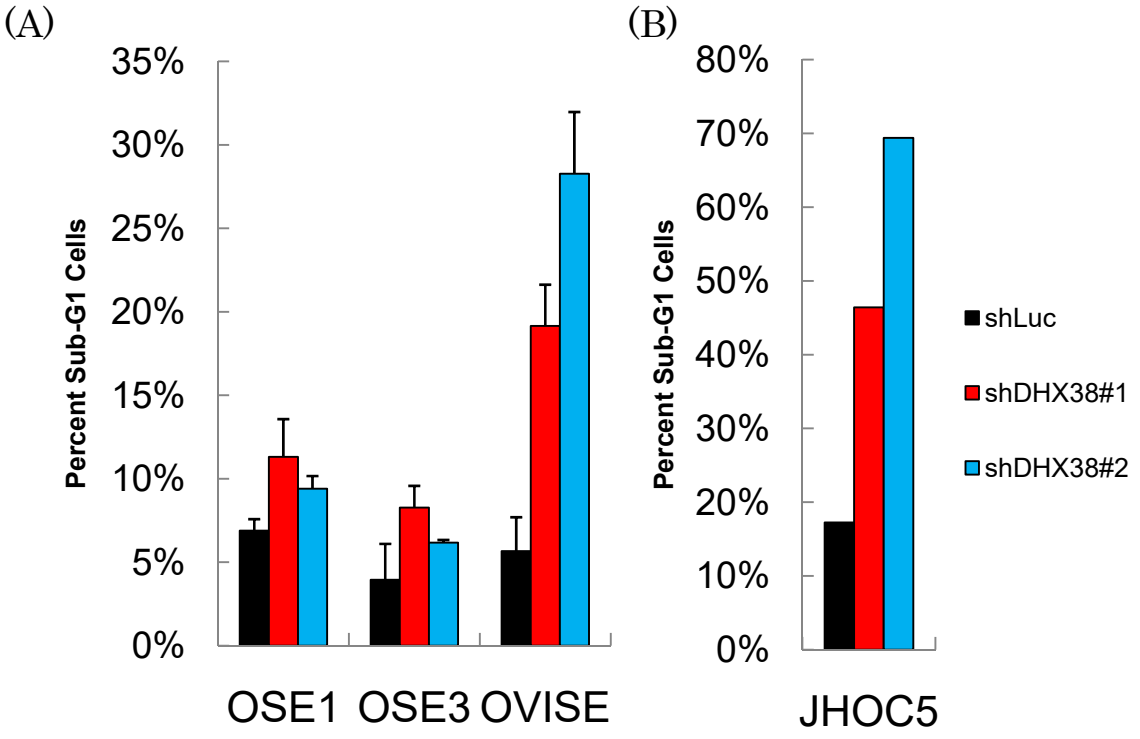

Figure 11. Knockdown of DHX38 via shRNA induces an OCCC-specific increase in Sub-G1 cells. After infection with a lentivirus containing the indicated shRNA, cells were cultured for 4 (A) or 5 (B) days, and fixed in a 70:30 ethanol:water solution at -20°C overnight. Cells were then stained with a propidium iodide solution and sub-G1 cells were measured via FACS. n = 2 (A); n = 1 (B).

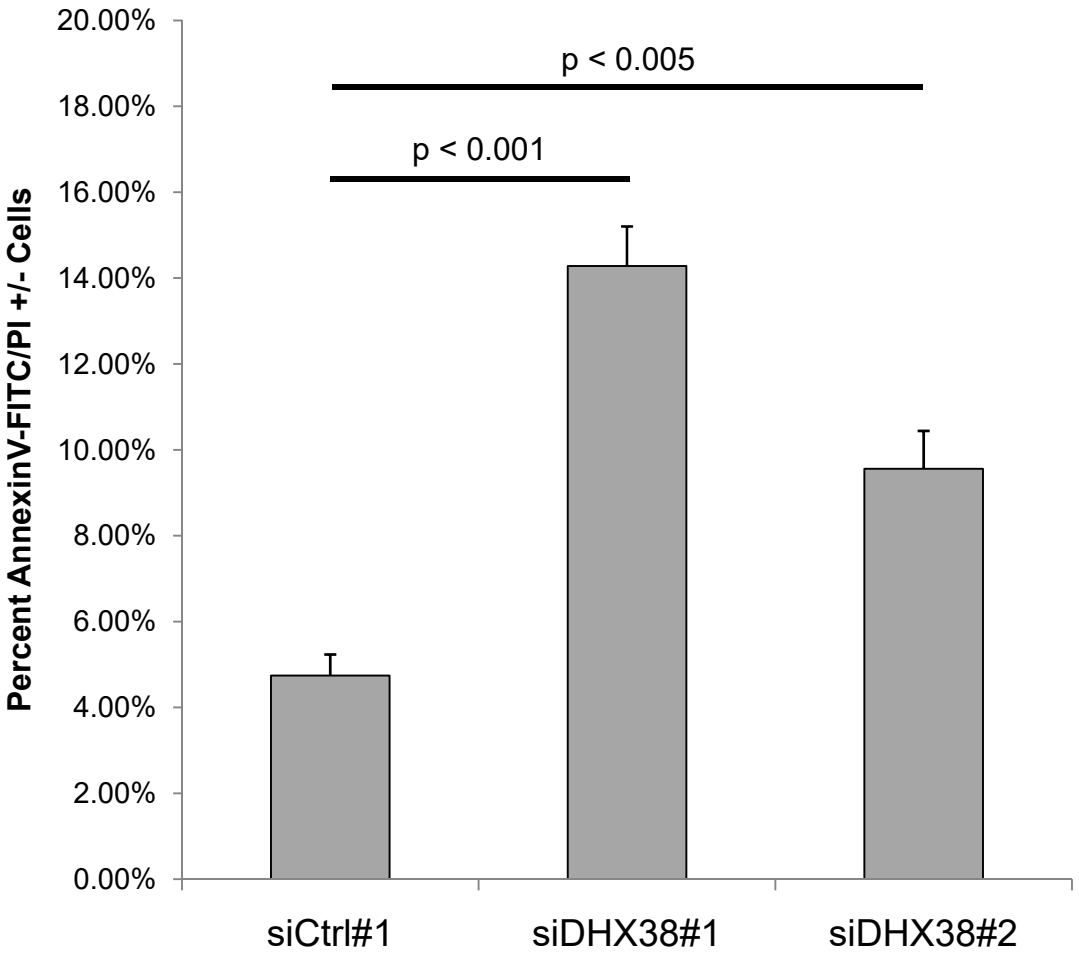

Figure 12. Knockdown of DHX38 increases the percentage of AnnexinV-FITC/PI +/- TOV21G cells. Four days after TOV21G cells were transfected with either a control siRNA or an siRNA targeting DHX38, cells were collected and analyzed via FACS. Data is displayed as the percent of cells positive for AnnexinV-FITC and negative for PI staining. (p-values calculated via student's t-test).

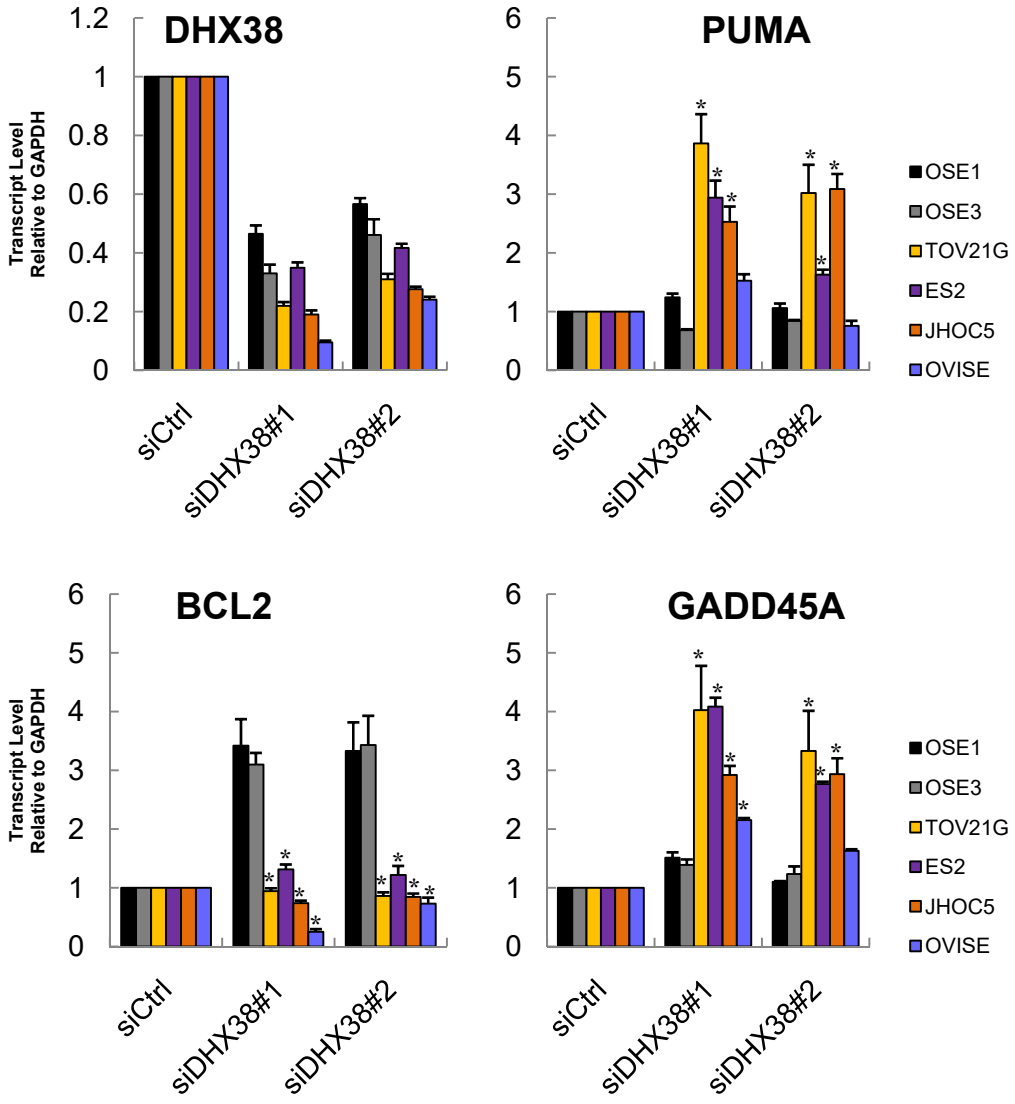

Figure13. siRNA-mediated knockdown induces transcriptional upregulation of pro-apoptotic genes in OCCC and anti-apoptotic genes in OSE. Transcript levels of the indicated genes relative to GAPDH was determined after treatment of cells (black bars represent OSE1, grey bars represent OSE3, orange bars represent TOV21G, and purple bars represent ES2) for 4 days with either a control siRNA or an siRNA directed against DHX38 ($n \geq 3$; *, $p < 0.05$ compared to both OSE1 and OSE3; unpaired student's t-test).

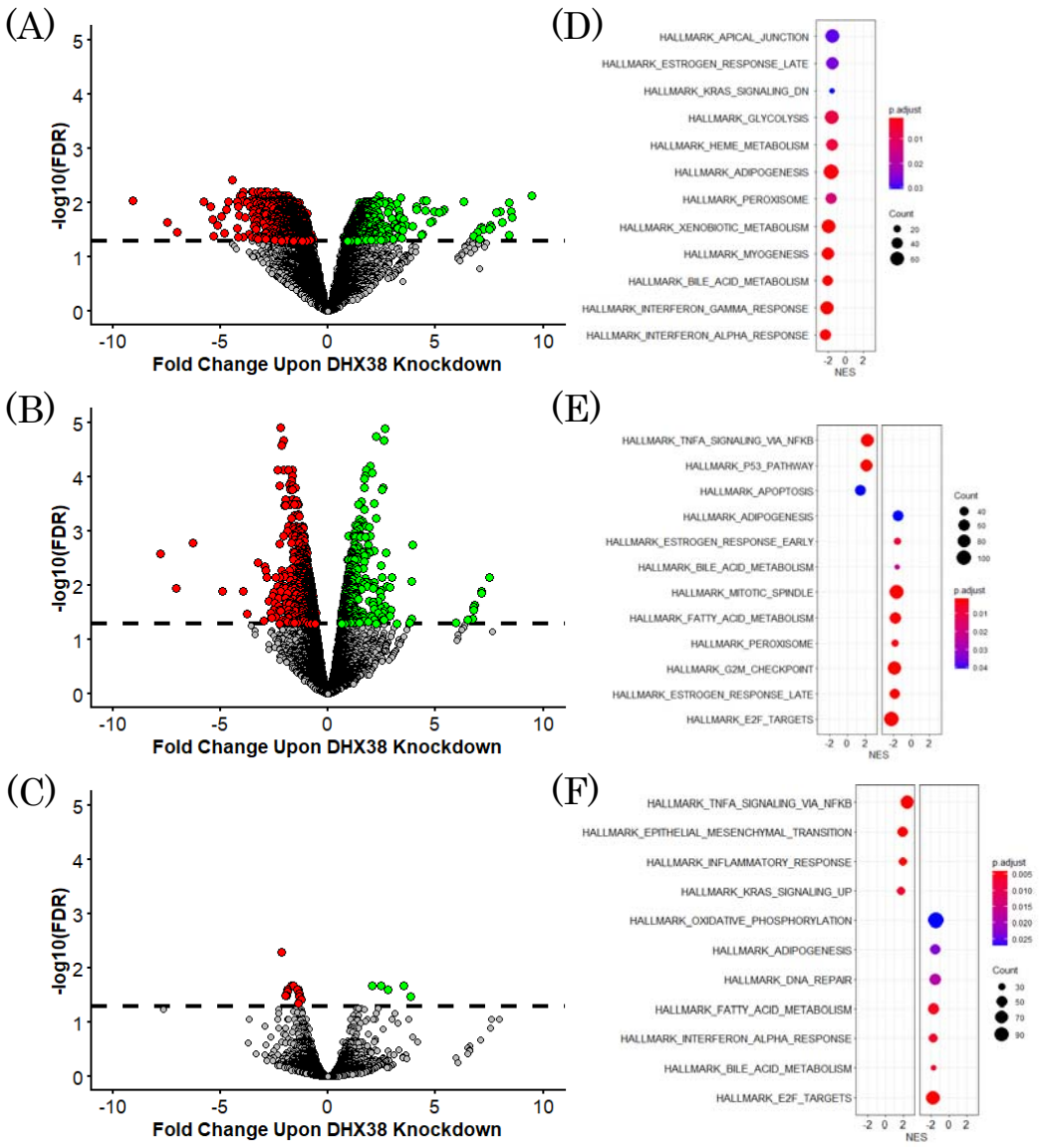

Figure 14. RNA-seq analysis uncovers pathways underlying DHX38 dependency in OCCC. Volcano plots of differentially expressed genes in (A) OSE3, (B) TOV21G, and (C) ES2 cell lines upon siRNA-mediated knockdown of DHX38. Dashed line represents FDR ≤ 0.05. Results of GSEA analysis on differentially expressed genes in (D) OSE3, (E) TOV21G, and (F) ES2.

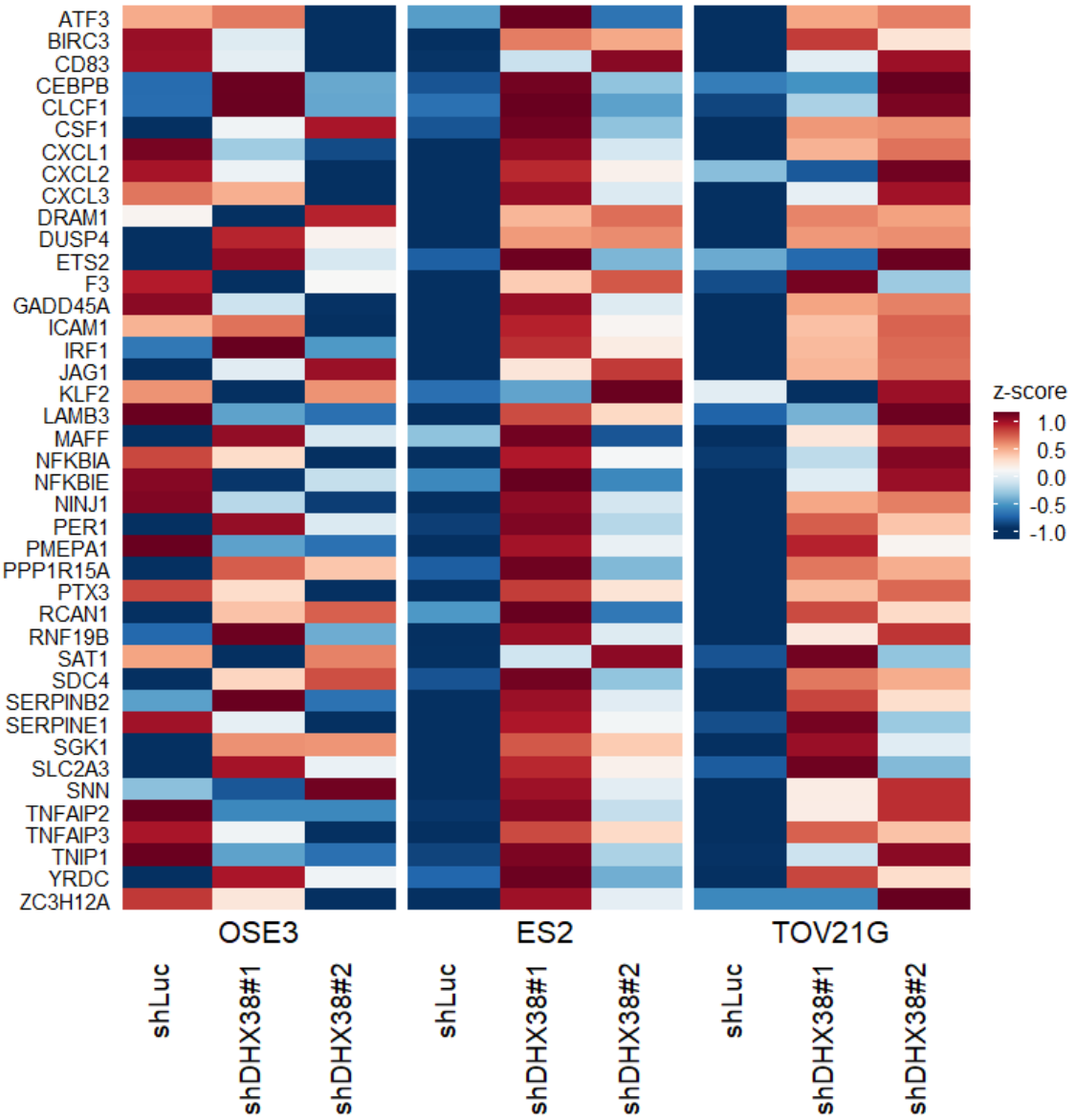

Figure 15. Expression heatmap of overlapping TOV21G and ES2 core enrichment genes from the HALLMARK_TNFA_SIGNALLING_VIA_NFKB gene set.

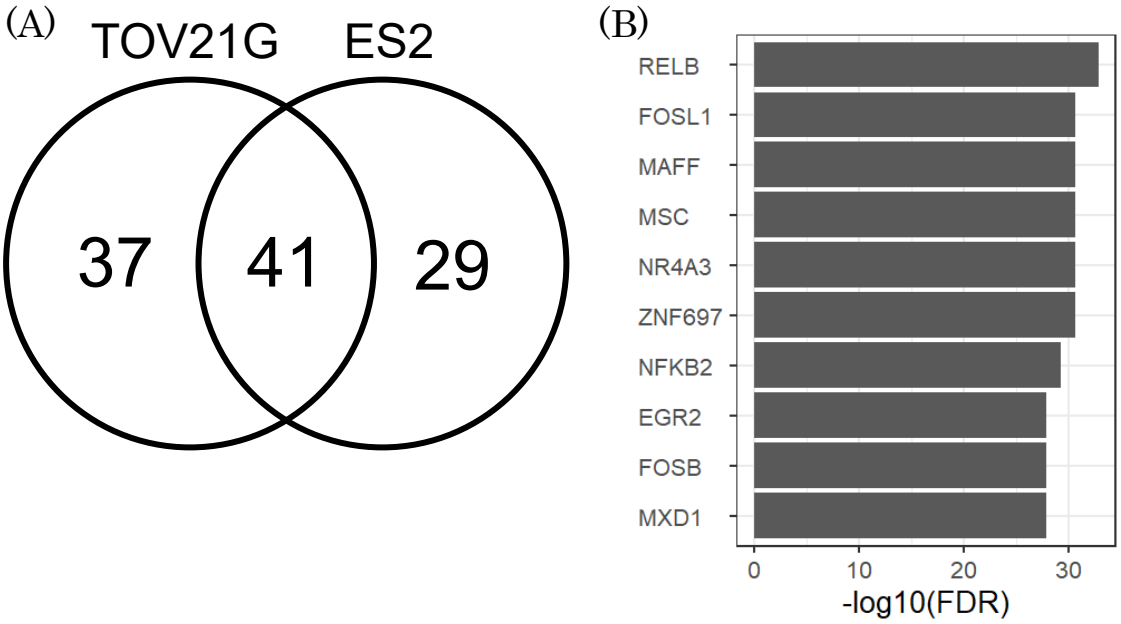

Figure 16. Analysis of HALLMARK_TNFA_SIGNALLING_VIA_NFKB hit genes. (A) Venn diagram of core pathway genes identified via GSEA for the differential expression data from the indicated cell lines. (B) Top transcription factors identified using the ChEA3 tool on common core pathway genes using the enrichr dataset.

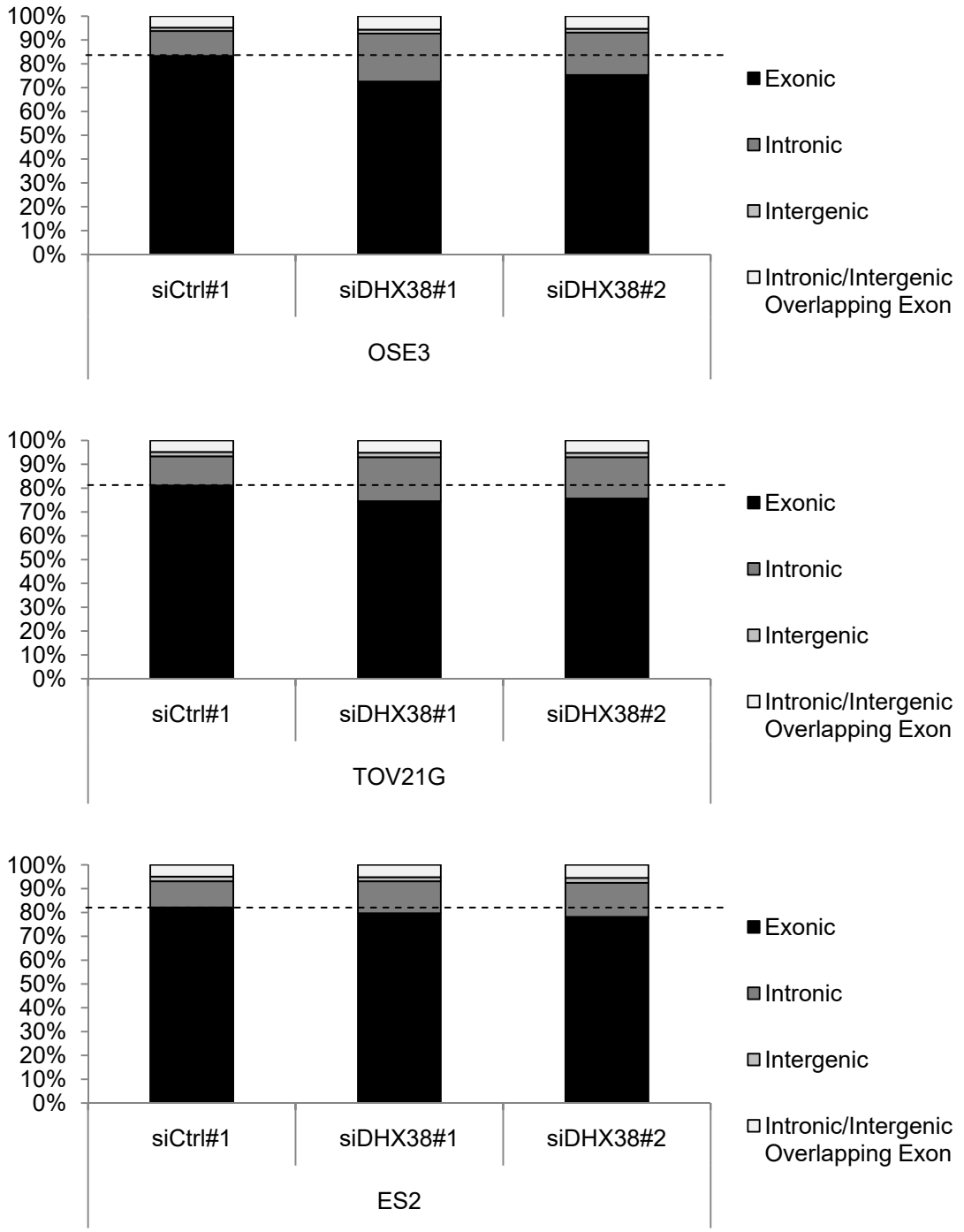

Figure 17. Profile of reads from RNA-seq mapped to each of the indicated genomic regions.

Concluding Remarks

In the current thesis, I endeavored to uncover and characterize genes whose knockdown in OCCC results in the attenuation of cell growth.Being particularly prevalent in Asia, the development of novel therapeutics – and therefore the search for novel therapeutic targets – against OCCC is of critical importance. I was able not only to successfully identify DHX38 as a growth dependency both in vitro and employing a mouse xenograft model using OCCC cell lines, but also demonstrate that its knockdown in normal OSE cells does not lead to a similar attenuation in growth. Additionally, the siRNA validation experiments I conducted using A549 and PC3 demonstrated the potential applicability of DHX38 as a therapeutic target in both lung and prostate carcinomas.

The functional characterization I next performed against DHX38 in OCCC and OSE cell lines demonstrated that knockdown of DHX38 in OCCC cells, but not OSE cells, leads to the induction of apoptosis in a p53-independent manner. While further studies will need to be carried out in order to better understand how knockdown of DHX38 leads to the induction of apoptosis, I was able to obtain preliminary results via RNA-seq that would suggest that knockdown of DHX38 in OCCC cells leads to the induction of the RelB signaling cascade. This signaling cascade is known in part for regulating the activity of the canonical NFκβ signaling pathway, whose upregulation is commonly observed in OCCC. Additionally, while DHX38 has been shown to localize to the spliceosome and is thought to play a role in branch point selection, the downstream effects of its knockdown on splicing are yet to be determined. With that in mind, I was also able to detect a global change in splicing upon knockdown of DHX38

via RNA-seq.

The work undertaken in this thesis has laid the groundwork for the understanding of the role DHX38 plays in OCCC, and has demonstrated the promise DHX38 holds as a potential new therapeutic target for the treatment of OCCC.

References

1. Acehan, D., Jiang, X., Morgan D. G., Heuser, J. E., Wang, X., and Akey, C. W. (2002). Three-Dimensional Structure of the Apoptosome: Implications for Assembly, Procaspase-9 Binding, and Activation. Mol. Cell *9*(2), 423-432.
2. Ajmal, M., Khan, M. I., Neveling, K., Khan, Y. M., Azam, M., Waheed, N. K., Hamel, C. P., Ben-Yosef, T., De Baere, E., Koenekoop, R. K., Collin, R. W., Qamar, R., and Cremers, F. P. (2014). A missense mutation in the splicing factor gene DHX38 is associated with early-onset retinitis pigmentosa with macular coloboma. J. Med. Genet. *51*(7), 444–448.
3. Anglesio M. S., Carey, M. S., Kobel, M., Mackay, H., Huntsman, D. G., and Vancouver Ovarian Clear Cell Symposium Speakers. (2011). Clear Cell Carcinoma of the Ovary: A Report From the First Ovarian Clear Cell Symposium, June 24th, 2010. Gynecol. Oncol. *121*(2), 407-415.
4. Ben-Hur, V., Denichenko, P., Siegfried, Z., Maimon, A., Krainer, A., Davidson, B., and Karni, R. (2013). S6K1 Alternative Splicing Modulates its Oncogenic Activity and Regulates mTORC1. Cell Rep. *3*(1), 103-115.
5. Billen, L. P., Kokoski, C. L., Lovell, J. F., Leber, B., and Andrews, D. W. (2008). Bcl-XL Inhibit Membrane Permeabilization by Competing with Bax. PLos Biol. *6*(6), e147.
6. Bitler, B. G., Wu, S., Park, P. W., Hai, Y., Aird, K. M., Wang, Y., Zhai, Y., Kossenkov, A. V., Vara-Ailor, A., Rauscher, III, F. J., et al. (2018). ARID1A-mutated ovarian cancers depend on HDAC6 activity. Nat. Cell Biol. *19*(8), 962-973.
7. Bode, A. M. and Dong, Z. (2004). Post-Translational Modification of p53 in Tumorigenesis. Nat. Rev. Cancer *4*, 793-805.

8. Bracken, A. P., Brien, G. L., and Verrijzer, C. P. (2019). Dangerous Liaisons: Interplay Between SWI/SNF, NuRD, and Polycomb in Chromatin Regulation and Cancer. Genes Dev. *33*(15-16), 936-959.

9. Chandler, R. L., Damrauer, J. S., Raab, J. R., Schisler, J. C., Wilkerson, M. D., Didion, J. P., Starmer, J., Serber, D., Yee, D., Xiong, J., et al. (2015). Coexistent ARID1A-PIK3CA mutations promote ovarian clear-cell tumorigenesis through pro-tumorigenic inflammatory cytokine signaling. Nat. Commun. *6*, 6118.

10. Chehab, N. H., Malikzay, A., Stavridi, E. S., and Halazonetis, T. D. (1999). Phosphorylation of Ser-20 Mediates Stabilization of Human p53 in Response to DNA Damage. Proc. Natl. Acad. Sci. USA *96*(24), 13777-13782.

11. Crotzer, D. R., Sun, C. C., Coleman, R. L., Wolf, J. K., Levenback, C. F., and Gershenson, D. M. (2007). Lack of Effective Systematic Therapy for Recurrent Clear Cell Carcinoma of the Ovary. Gynecol. Oncol. *105*(2), 404-408.

12. Das, S., Anczuków, O., Akerman, M., and Krainer, A. R. (2012). Oncogenic Splicing Factor SRSF1 is a Critical Transcriptional Target of MYC. Cell Rep. *1*(2), 110-117.

13. Dempster, J. M., Rossen, J., Kazachkova, M., Pan, J., Kugener, G., Root, D. E., and Tsherniak, A. (2019). Extracting Biological Insights from the Project Achilles Genome-Scale CRISPR Screens in Cancer Cell Lines. Biorxiv 720243.

14. Fraile, J. M., Manchado, E., Lujambio, A., Quesada, V., Campos-Iglesias, D., Webb, T. R., Lowe, S. W., López-Otín, C., and Freije, J. M. P. (2017). USP39 Deubiquitinase Is Essential for KRAS Oncogene-driven Cancer. J. Biol. Chem. *292*(10), 4164-4175.

15. Hamada, T., Nowak, J. A., and Ogino, S. (2017). PIK3CA mutation and colorectal cancer precision medicin. Oncotarget. *8*(14), 22305-22306.

16. Han, S., Park, J., and Lee, D. H. (2015). Protein DHX38 is a novel inhibitor of protein phosphatase 4. Anim. Cells Sys. *19*(4), 236-244.

17. Haupt, Y., Maya, R., Kazaz, A., and Oren, M. (1997). Mdm2 Promotes the Rapid Degradation of p53. Nature *387*(6630), 296-299.

18. Hegele, A., Kamburov, A., Grossmann, A., Sourlis, C., Wowro, S., Weimann, M., Will, C. L., Pena, V., Lührmann, R., and Stelzl, U. (2012). Dynamic Protein-Protein Interaction Wiring of the Human Spliceosome. Mol. Cell *45*(4), 567-580.

19. Hemann, M. T. and Lowe, S. W. (2006). The p53-Bcl-2 Connection. Cell Death Diff. *13*, 1256-1259.

20. Hsu, H., Xiong, J., and Goeddel, D. (1995). The TNF Receptor 1-Associated Protein TRADD Signals Cell Death and NF- κ B Activation. Cell *81*, 495-504.

21. Hsu, T. Y., Simon, L. M., Neill, N., Marcotte, R., Sayad, A., Bland, C. S., Echeverria, G. V., Sun, T., Kurley, S. J., Tyagi, S., et al. (2015). The Spliceosome is a Therapeutic Vulnerability in MYC-driven Cancer. Nature *525*(7569), 384-388.

22. Ito, A., Lai, C. H., Zhao, X., Saito, S., Hamilton, M. H., Appella, E., and Yao, T. P. (2001). p300/CBP-mediated p53 acetylation is commonly induced by p53-activating agents and inhibited by MDM2. Embo. J. *20*(6), 1331-1340.

23. Johnson, J. M., Castle, J., Garrett-Engele, P., Kan, Z., Loerch, P. M., Armour, C. D., Santos, R., Schadt, E. E., Stoughton, R., and Shoemaker, D. D. (2003). Genome-Wide Survey of Human Alternative Pre-mRNA Splicing with Exon Junction Microarrays. Science *302*(5653), 2141-2144.

24. Kale, J., Osterlund, E. J., and Andrews, D. W. (2018). BCL-2 Family Proteins: Changing Partners in the Dance Toward Death. Cell Death Diff. *25*, 65-80.

25. Karin, M. (1999). How NF-kB is Activated: the Role of the IkB Kinase (IKK) Complex. Oncogene *18*, 6867-6874.

26. Keenan, A. B., Torre, D., Lachmann, A., Leong, A. K., Wojciechowicz, M. L., Utti, V., et al. (2019). ChEA3: transcription factor enrichment analysis by orthogonal omics integration. Nuc. Acids Res. *47*(W1), W212-W224.

27. Kim, H., Park, C. K., Lee, S. J., Rha, S. Y., Park, K. H., and Lim, H. Y. (2013). PIK3CA Mutations in Hepatocellular Carcinoma in Korea. Yonsei Med. J. *54*(4), 883-887.

28. Ku, F. C., Wu, R. C., Yang, L. Y. ,Tang, Y. H., Chang, W. Y. Yang, J. E., Wang, C. C., Jung, S. M., Lin, C. T., Chang, T. C, et al. (2018). Clear Cell Carcinomas of the Ovary Have Poorer Outcomes Compared with Serous Carcinomas: Results from a Single-center Taiwanese Study. J. Formosan Med. Assoc. *117*(2), 117-125.

29. Kühnel, F., Zender, L., Paul, Y., Tietze, M. K., Trautwein, C., Manns, M., and Kubicka, S. (2000). NF κ B Mediates Apoptosis through Transcriptional Activation of Fas (CD95) in Adenoviral Hepatitis. JBC *275*, 6421-6427.

30. Latif, Z., Chakchouk, I., Schrauwen, I., Lee, K., Santos-Cortez, R., Abbe, I., Acharya, A., Jarral, A., Ali, I., Ullah, E., Khan, M. N., Ali, G., Tahir, T. H., Bamshad, M. J., Nickerson, D. A., Ahmad, W., Ansar, M., Leal, S. M., and University of Washington Center for Mendelian Genomics (UWCMG) Study Group (2018). Confirmation of the Role of DHX38 in the Etiology of Early-Onset Retinitis Pigmentosa. Ivest. Opthalmol. Vis. Sci. *59*(11), 4552–4557.

31. Li, W., Chen, Z., Zong, Y., Gong, F., Zhu, Y., Zhu, Y., Lv, J., Zhang, J., Xie, L., Sun, Y., et al. (2011). PP2A inhibitors induce apoptosis in pancreatic cancer cell line PANC-1 through persistent phosphorylation of IKKα and sustained activation of the NF-κB pathway. Cancer Letters *304*(2), 117-127.

32. Li, W., Xu, H., Xiao, T., Cong, L., Love, M. I., Zhang, F., Irizarry, R. A., Liu, J. S., Brown, M., and Liu, X. D. (2014). MAGeCK Enables Robust Identification of Essential Genes from Genome-Scale CRISPR/Cas9 Knockout Screens. Gen. Biol. *15*, 554.

33. Li, X., Zhao, Y., Xia, Q., Zheng, L., Liu, L., Zhao, B., and Jing, S. (2016). Nuclear Translocation of Annexin 1 Following Oxygen-Glucose Deprivation-reperfusion Induces Apoptosis by Regulating Bid Expression Via p53 Binding. Cell Death Dis. *7*, e2356.

34. Liberzon, A., Birger, C., Thorvaldsdóttir, H., Ghandi, M., Mesirov, J. P., and Tamayo, P. (2015). The Molecular Signatures Database (MSigDB) hallmark gene set collection. Cell Syst. *1*(6), 417-425.

35. Lindeonboim, L., Borner, C., and Stein, R. (2001). Bcl-x_s can form homodimers and heterodimers and its apoptotic activity requires localization of Bcl-x_s to the mitochondria and its BH3 and loop domains. Cell Death Diff. *8*, 933-942.

36. Liu, P., Wang, Y., and Li, X. (2019). Targeting the Untargetable KRAS in Cancer Therapy. APSB *9*(5), 871-879.

37. Ma, Y., Barnett, T., Chai, L., Yang, J., Alipio, Z., Pei, L., Amin, H. M., Fink, L., Di, C., Yan, H., and Ward, D. (2006). DEAH-Box Splicing Factor Gene, Prp16 Amplification in Acute Myeloid Leukemia. Blood *108*(11), 4779.

38. Mabuchi, S., Sugiyama, T., and Kimura, T. (2016). Clear Cell Carcinoma of the Ovary: Molecular Insights and Future Therapeutic Perspectives. J. Gynecol. Oncol. *27*(3), e31.

39. Matos, P. and Jordan, P. (2006). Rac1, but not Rac1B, Stimulates RelB-mediated Gene Transcription in Colorectal Cancer Cells. JBC *281*, 13724-13732.

40. McCarthy, D. J., Chen, Y., and Smyth, G. K., (2012). Differential expression analysis of multifactor RNA-Seq experiments with respect to biological variation. Nuc. Acids Res. *40*(10), 4288-4297.

41. McNeill, R. S., Stroobant, E. E., Smithberger, E., Canoutas, D. A., Butler, M. K., Shelton, A. K., Patel, S. D., Limas, J. C., Skinner, K. R., Bash, R. E., et al. (2018). PIK3CA missense mutations promote glioblastoma pathogenesis, but do not enhance targeted PI3K inhibition.

42. Meyers, R. M., Bryan, J. G., McFarland, J. M., Weir, B. A., Sizemore, A. E., Xu, H., Dharia, N. V., Montgomery, P. G., Cowley, G. S., Pantel, S., et al. (2017). Computational Correction of Copy Number Effect Improves Specificity of CRIPSR-Cas9 Essentiality Screens in Cancer Cells.

43. Mi, H., Dong, Q., Muruganujan, A., Gaudet, P., Lewis, S., and Thomas, P. D. (2010). PANTHER version 7: Improved Phylogenetic Trees, Orthologs and Collaboration with the Gene Ontology Consortium. Nucl. Acids Res. *38*, D204-D210.

44. Michael, D. and Oren, M. (2003). The p53-Mdm2 Module and the Ubiquitin System. Semin. Cancer Biol. *13*(1), 49-58.

45. Mosele, F., Stefanovska, B., Lusque, A., Dien, T. A., Garberis, I., Droin, N., Le Tourneau, C., Sablin, M.-P., Lacroix, L., Enrico, D., et al. (2020). Outcome and Molecular Landscape of Patients with PIK3CA-mutated Metastatic Breast Cancer. Ann. Onc. *31*(3), 377-386.

46. Nagata, S. (1997). Apoptosis by Death Factor. Cell *8*(3), 355-365.

47. Ott, M., Robertson, J. D., Gogvadze, V., Zhivotovsky, B., and Orrenius, S. (2002). Cytochrome c Release from Mitochondria Proceeds by a Two-Step Process. PNAS *99*(3), 1259-1263.

48. Pangallo, J., Kiladjian, J., Cassinat, B., Renneville, A., Taylor, J., Polaski, J. T., North, K., Abel-Wahab, O., and Bradley, R. K. (2020). Rare are Private Spliceosomal Gene Mutations Drive Partial, Complete, and Dual Phenocopies of Hotspot Alterations. Blood *135*(13), 1032-1043.

49. Paronetto, M. P., Achsel, T., Massiello, A., Chalfant, C. E., and Sette. C. (2007). The RNA-Binding Protein Sam68 Modulates the Alternative Splicing of Bcl-x. J. Cell Biol. *176*(7), 929-939.

50. Rauch, J., Moran-Jones, K., Albrecht, V., Schwarzl, T., Hunter, K., Gires, O., and Kolch, W. (2011). c-Myc Regulates RNA Splicing of the A-Raf Kinase and its Activation of the ERK Pathway.Cancer Res. *71*(13), 4664-4674.

51. Robinson, M. D., McCarthy, D. J., and Smyth, G. K. (2010). edgeR: a Bioconductor package for differential expression analysis of digital gene expression data. Bioinformatics *26*(1), 139-140.

52. Samartzis, E. P., Gutsche, K., Dedes, K. J., Fink, D., Stucki, M., and Imesch, P. (2014). Loss of ARID1A expression sensitizes cancer cells to PI3K- and AKT-inhibition. Oncotarget*5*, 5295-5303.

53. Sanjana, N. E., Shalem, O., and Zhang, F. (2014). Improved Vectors and Genome-Wide Libraries for CRISPR Screening. Nat. Methods *11*(8), 783-784.

54. Semlow, D. R., Blanco M. R., Walter, N. G., and Staley, J. P. (2016). Spliceosomal DEAH-Box ATPases Remodel Pre-mRNA to Activate Alternative Splice Sites. Cell *164*(5), 985-998.

55. Sen, N., Hara, M. R., Kornberg, M. D., Cascio, M. B., Bae, B. I., Shahani, N., Thomas, B., Dawson, T. M., Dawson, V. L., Snyder, S. H., et al. (2008). Nitric Oxide-induced Nuclear GAPDH Activates p300/CBP and Mediates Apoptosis. Nat. Cell Biol. *10*, 866-873.

56. Shalem, O., Sanjana, N. E., Hartenian, E., Shi, X., Scott, D. A., Mikkelson, T., Heckl, D., Ebert, B. L., Root, D. E., Doench, J. G., et al. (2014). Genome-Scale CRISPR-Cas9 Knockout Screening in Human Cells. Science *343*(6166), 84-87.

57. Shao, D. D., Xue, W., Krall, E. B., Bhutkar, A., Piccioni, F., Wang, X., Schinzel, A. C., Sood, S., Rosenbluh, J., Kim, J. W., et al. (2014). KRAS and YAP1 converge to regulate EMT and tumor survival. Cell *158*(1), 171-184.

58. Shen, J., Peng, Y., Wei, L., Zhang, W., Yang, L., Lan, P. Kapoor, P., Ju, Z., Mo, Q., Shih, I., et al. (2015). ARID1A Deficiency Impairs the DNA Damage Checkpoint and Sensitizes Cells to PARP Inhibitors. Cancer Disc. *5*(7), 752-767.

59. Singh, A., Greninger, P., Rhodes, D., Koopman, L., Violette, S., Bardeesy, N., Settleman, J. Cancer Cell *15*(6), 489-500.

60. Subramanian, A., Tamayo, P., Mootha, V. K., Mukherjee, S., Ebert, B. L., Gillete, M. A., et al. (2005). Gene set enrichment analysis: A knowledge-based approach for interpreting genome-wide expression profiles.

61. Sugiyama, T., Kamura, T., Kigawa, J., Terakawa, N., Kikuchi, Y., Kita, T., Mitsuaki, S., Sato, I, and Taguchi, K. (2000). Clinical Characteristics of Clear Cell Carcinoma of the Ovary. Cancer *88*(11), 2584-2589.

62. Sun, H., Yang, T., Zang, W., and Wu, S. (2010). Dehydroepiandrosterone-induced proliferation of prostatic epithelial cell is mediated by NFKB via PI3K/AKT signaling pathway. J. Endocrinol. *204*(3), 311-318.

63. Tang, H., Liu, Y., Wang, X., Guan, L., Chen, W., Jiang, H., and Lu, Y. (2018). Clear Cell Carcinoma of the Ovary Clinicopathologic Features and Outcomes in a Chinese Cohort. Medicine. *97*(21), e10881.

64. Tate, J. G., Bamford, S., Jubb, H. C., Sondka, Z., Beare, D. M., Bindal, N., Boutselakis, H., Cole, C. G., Creatore, C., Dawson, E., et al. (2018). COSMIC: the Catalogue of Somatic Mutations in Cancer. Nuc. Acid Res. *47*(D1), D941-D947.

65. Thomas, P. D., Campbell, M. J., Kejariwal, A., Mi, H., Karlak, B., Daverman, R., Diemer, K., Muruganujan, A., and Narechania, A. (2003). PANTHER: A Library of Protein Families and Subfamilies Indexed by Function. Genome Res. *13*, 2129-2141.

66. Tseng, C. H., Liu H. L., and Cheng, S. C. (2011). DEAH-box ATPase Prp16 Has Dual Roles in Remodeling of the Spliceosome in Catalytic Steps. RNA *17*, 145-154.

67. Watanabe, R., Ui, A., Kanno, S., Ogiwara, H., Nagase, T., Kohno, T., and Yasui, A. (2014). SWI/SNF Factors Required for Cellular Resistance to DNA Damage Include ARID1A and ARID1B and Show Interdependent Protein Stability. Mol. Cell Pathobiol. *74*(9), 2465-2475.

68. Yamamoto, H., Shigematsu, H., Nomura, M., Lockwood, W. W., Sato, M., Okumura, N., Soh, J., Suzuki, M., Witsuba, I. I., Fong, K. M., et al. (2010). PIK3CA Mutations and Copy Number Gains in Human Lung Cancers. Cancer Res. *68*(17), 6913-6921.

69. Yang, J., Nie, J., Ma, X., Wei, Y., Peng, Y., and Wei, X. (2019). Targeting PI3K in cancer: mechanisms and advances in clinical trials. Mol. Cancer *18*, 26.

70. Zhu, Z., Golay, H. G., and Barbie, D. A. (2014). Targeting Pathways Downstream of KRAS in Lung Adenocarcinoma. Pharmacogenomics *15*(11), 1507-1518.

Acknowledgements

First and foremost, I would like to thank Professors Kobayashi Takehiko and Tetsu Akiyama for their support and encouragement over the course of my studies here at the University of Tokyo. I would also like to thank Dr. Tomoatsu Hayashi and Dr. Takeaki Oda for their guidance and mentorship, and together with Dr. Kawasaki Yoshihiro and Dr. Yamazumi Yusuke for their technical advice and many stimulating discussions. In addition, I would also like to thank Dr. Suda Sakiko for her assistance with performing experiments, and Dr. Nagayoshi Yoko and Dr. Kamoshida Yuki for always helping to give the lab a lively atmosphere, and for many late-night discussions.

I would also like to thank my family and friends for their continuous support throughout my time here at the University of Tokyo.

Brandon James Cona